**Article:**

eprints@whiterose.ac.uk
https://eprints.whiterose.ac.uk/

1 **Olfactory rod cells: a rare cell type in the larval zebrafish olfactory epithelium**

2 **with an actin-rich apical projection**

3

4 King Yee Cheung[1], Suresh J. Jesuthasan[2,3,*], Sarah Baxendale[1], Nicholas J. van

5 Hateren[1], Mar Marzo[1], Christopher J. Hill[1] and Tanya T. Whitfield[1,*]

6

7 [1]Department of Biomedical Science, University of Sheffield, Sheffield, S10 2TN, UK

8 [2]Lee Kong Chian School of Medicine, Nanyang Technological University, Singapore

9 [3]Institute of Molecular and Cell Biology, Singapore

10

11 *Authors for correspondence:

12 Tanya T. Whitfield

13 t.whitfield@sheffield.ac.uk,

14

15 Suresh J. Jesuthasan

16 sureshjj@imcb.a-star.edu.sg

17

18 **Author ORCIDs:**

19 King Yee Cheung 0000-0002-1098-4926

20 Suresh J. Jesuthasan 0000-0002-5733-6555

21 Sarah Baxendale 0000-0002-6760-9457

22 Nicholas J. van Hateren 0000-0002-0011-9947

23 Mar Marzo 0000-0003-1591-0309

24 Christopher J. Hill 0000-0002-6914-4411

25 Tanya T. Whitfield 0000-0003-1575-1504

26

27 **Key words:** olfactory rod cell, olfactory placode, olfactory epithelium, actin, actin-rich

28 projection, Lifeact, zebrafish

29

30 **Abstract**

31 We report the presence of a rare cell type, the olfactory rod cell, in the developing

32 zebrafish olfactory epithelium. These cells each bear a single actin-rich rod-like

33 apical projection extending about 10 µm from the epithelial surface. Live imaging

34 with a ubiquitous Lifeact-RFP label indicates that the rods can oscillate. Olfactory

35 rods arise within a few hours of the olfactory pit opening, increase in numbers and

36 size during larval stages, and can develop in the absence of olfactory cilia. Olfactory

37 rod cells differ in morphology from the known classes of olfactory sensory neuron,

38 but express reporters driven by neuronal promoters. The cells also differ from

39 secondary sensory cells such as hair cells of the inner ear or lateral line, or sensory

40 cells in the taste bud, as they are not associated with established synaptic terminals.

41 A sub-population of olfactory rod cells expresses a Lifeact-mRFPruby transgene

42 driven by the *sox10* promoter. Mosaic expression of this transgene reveals that

43 olfactory rod cells have rounded cell bodies located apically in the olfactory

44 epithelium.

45

46  **Introduction**

47  The vertebrate olfactory epithelium (OE) enables the detection of chemical cues,

48  giving rise to the sense of smell (reviewed in [Axel, 1995]). The function of this

49  epithelium, which derives from paired cranial neurogenic placodes, is mediated by a

50  diverse set of cells that includes neuronal receptors and non-sensory cells. Olfactory

51  sensory neurons (OSNs) are bipolar neurons that extend a dendrite to the apical

52  surface of the OE, and an axon to the olfactory bulb (OB). In mammals, two broad

53  classes of sensory receptors — ciliated and microvillous OSNs — have been

54  identified on the basis of morphology, receptor expression and OB target.

55  Mammalian OSNs can act as both chemosensors and mechanosensors (Grosmaitre

56  et al., 2007; Iwata et al., 2017). The OE of other vertebrates also contains ciliated

57  and microvillous neurons. In fish, additional classes of OSNs have been identified.

58  Each occupies a stereotyped position within the pseudostratified OE, with the

59  dendrite bearing a distinct and characteristic specialisation projecting into the

60  environment (Hansen & Zeiske, 1998; Hansen & Zielinski, 2005; Sato et al., 2005;

61  reviewed in [Maier et al., 2014]).

62

63  In zebrafish, ciliated neurons, which express olfactory marker protein (OMP) and

64  odorant receptor (OR) genes, have a cell body that lies deep within the OE, an axon

65  that projects to dorsal and medial regions of the OB, and a slender dendrite

66  extending to the surface of the olfactory pit. Here, the dendritic knob bears a cluster

67  of primary cilia that project into the olfactory cavity (Hansen & Zeiske, 1998; Hansen

68  & Zielinski, 2005; Sato et al., 2005). Microvillous neurons, characterised by the

69  expression of TrpC2 and vomeronasal (VR)-type pheromone receptors, have cell

70  bodies that lie in the intermediary layer of the OE, an axon that projects to the lateral

71  part of the OB, and a dendrite bearing a tuft of short, actin-rich microvilli (Hansen &

72  Zeiske, 1998; Hansen & Zielinski, 2005; Sato et al., 2005). Crypt neurons, less

73  abundant than ciliated or microvillous neurons, have rounded cell bodies that sit

74  apically in the OE, with both cilia and microvilli extending from a crypt within the cell

75  body (Hansen & Zeiske, 1998; Hansen & Zielinski, 2005; Parisi et al., 2014; Biechl et

76  al., 2016; Bettini et al., 2017). Kappe neurons lie in the superficial layers of the adult

77  zebrafish OE and are named for their apical actin-rich cap, presumed to be microvilli

78  (Ahuja et al., 2014). Pear-shaped neurons are also positioned superficially in the

79    adult OE and have short apical dendrites, but express some markers in common

80    with ciliated neurons (Wakisaka et al., 2017).

81

82    OSNs are surrounded and separated by a network of non-neuronal cell types. These

83    include sustentacular (support) cells, basal cells that replenish the OSNs, and goblet

84    cells that produce mucus (Hansen & Zeiske, 1993; Hansen & Zeiske, 1998; reviewed

85    in [Olivares & Schmachtenberg, 2019]; Demirler et al., 2019). In fish, multiciliated

86    cells, located around the rim of the olfactory pit, each bear multiple long motile cilia.

87    These have a characteristic 9+2 axoneme and beat at around 24 Hz, resulting in an

88    asymmetric flow that draws water and odorants into the olfactory cavity and flushes

89    them out again (Reiten et al., 2017).

90

91    In addition to common cell types, tissues may also contain rare or sparsely-

92    distributed cell types, which are difficult to detect by conventional histological

93    methods. These include stem cells, immune cells, or other rare cell types, which can

94    have critical functions (see, for example, [Montoro et al., 2018; Sui et al., 2018]).

95    Characterisation of the identity and lineage of every cell type of an organ system is a

96    goal of many contemporary single-cell and single-nucleus RNA-seq studies (Junker

97    et al., 2014; Satija et al., 2015; Hernández et al., 2018; Raj et al., 2018; Farnsworth

98    et al., 2020; Wattrus & Zon, 2020). Transgenic or other fluorescent markers, coupled

99    with high-resolution imaging of the whole embryo, can also help to identify cell types

100   that may previously have been overlooked (see, for example, [Kawakami et al.,

101   2010; Galanternik et al., 2017; van Lessen et al., 2017]).

102

103   We report here the existence of a rare cell type, the olfactory rod cell, in the

104   developing zebrafish OE. Olfactory rod cells are characterised by a single actin-rich

105   apical projection. The morphology of the rod matches brief descriptions of similar

106   structures in the OE of several other fish species, many of which were previously

107   dismissed either as senescent forms of OSNs or as fixation artefacts. Using a variety

108   of imaging techniques and transgenic lines, including live imaging, we show that

109   zebrafish olfactory rod cells are present in living fish and can be detected from early

110   stages of larval development.

111

112  **Materials and Methods**

113  ***Zebrafish husbandry***

114  Zebrafish strains used in this study were wild type (AB strain – ZFIN), *ift88[tz288b]*

115  (Tsujikawa & Malicki, 2004), *sox10[m618]* (Dutton et al., 2001), *Tg(actb2:Lifeact-*

116  *RFP)[e115]* (Behrndt et al., 2012), *Tg(actb2:Lifeact-GFP)[e114]* (Behrndt et al., 2012),

117  *Tg(Xla.Tubb:jGCaMP7f)[sq214]* (Chia et al., 2019), *Tg(elavl3:GCaMP6f)[jf1]* (Dunn et al.,

118  2016), *Tg(elavl3:H2B-GCaMP6s)[jf5]* (Dunn et al., 2016)*, Tg(pou4f3:GAP-GFP)[s356t]*

119  (Xiao et al., 2005) and *Tg(sox10:Lifeact-mRFPruby)[sh630]* (this study). Homozygous

120  *sox10^{-/-}* mutant larvae were identified by their lack of body pigmentation at 5 days

121  post-fertilisation (dpf). Adult zebrafish were kept in a 10 hours dark/14 hours light

122  cycle at 28.5°C and spawned by pair-mating or marbling (Aleström et al., 2019).

123  Eggs were collected and staged according to standard protocols (Kimmel et al.,

124  1995; Nüsslein-Volhard & Dahm, 2002), and raised in E3 medium (5 mM NaCl, 0.17

125  mM KCl, 0.33 mM $CaCl_2$, 0.33 mM $MgSO_4$, with 0.0001% methylene blue at early

126  stages) at 28.5°C. For controlling the developmental rate to obtain embryos at

127  stages 34-46 hours post-fertilisation (hpf), embryos were incubated at 25°C or 34°C

128  in accordance with Kimmel's formula, $H_T = h \div (0.055T - 0.57)$ (Kimmel et al.,

129  1995). For live imaging, zebrafish were anaesthetised with 0.5 mM tricaine mesylate

130  in E3.

131

132  ***Generation of the Tg(sox10:Lifeact-mRFPruby) transgenic line***

133  The *-4725sox10:Lifeact-mRFPruby* construct was generated using the Gateway Tol2

134  kit (Kawakami, 2007; Kwan et al., 2007). The p5E *-4725sox10* promoter (Dutton et

135  al., 2008; Rodrigues et al., 2012), pME-*Lifeact-mRFPruby* (Riedl et al., 2008), and

136  p3E polyA sequences were cloned into pDestTol2pA3 through an LR Clonase

137  reaction. The 12.1 kb final plasmid was sequenced and injected into the AB strain.

138  Injected embryos were grown to adulthood and crossed to AB. Transgenic progeny

139  from one founder male were selected based on mRFPruby expression in the inner

140  ear and grown to adulthood to generate a stable line. Embryos with bright

141  fluorescence, presumed to be homozygous for the transgene, were chosen for

142  imaging.

143

144  ***Immunohistochemistry and phalloidin staining***

145 Zebrafish embryos and larvae were fixed in 4% paraformaldehyde (PFA) in

146 phosphate-buffered saline (PBS) for two hours at room temperature or overnight at

147 4°C. Zebrafish were washed three or more times with PBS, and permeabilised by

148 incubation in PBS-Triton X-100 (0.2% Triton for 32-48 hpf embryos, 1% Triton for

149 later stages) for several hours at 4°C until staining.

150

151 To visualise F-actin, zebrafish were stained with either Alexa Fluor 488 phalloidin

152 (Cell Signaling Technology; 1:150), Alexa Fluor 568 (Invitrogen ThermoFisher; 1:50),

153 or Alexa Fluor 647 phalloidin (Invitrogen ThermoFisher; 1:50) in PBS overnight at

154 4°C. After staining, zebrafish were washed four times in PBS over two or more hours

155 before imaging.

156

157 For antibody staining, after fixing and washing, zebrafish were washed a further

158 three times in PBS-0.2% Triton and incubated in blocking solution (10% sheep

159 serum in PBS-0.2% Triton for acetylated α-tubulin staining; 1% bovine serum

160 albumin (BSA) in PBS-0.1% Triton for SV2 staining) for 60 minutes at room

161 temperature. Primary antibodies were mouse IgG1 anti-acetylated α-tubulin antibody

162 (Sigma-Aldrich; 1:100) and mouse IgG1 anti-SV2 antibody (deposited in

163 Developmental Studies Hybridoma Bank by K. M. Buckley; 1:100). Staining was

164 carried out in blocking solution containing 1% dimethyl sulfoxide (DMSO; Sigma-

165 Aldrich) overnight at 4°C. Zebrafish were washed three times in PBS-0.2% Triton,

166 and a further four times over two or more hours. The secondary antibody was Alexa

167 647-conjugated goat anti-mouse IgG1 (Invitrogen ThermoFisher; 1:200). For double

168 stains with phalloidin, Alexa Fluor 488 phalloidin (1:150) and DMSO (1%) were

169 added together with the secondary antibody in blocking solution overnight at 4°C.

170 Zebrafish were then washed four times in PBS-0.2% Triton and stored at 4°C until

171 imaging. Controls with no primary antibody yielded no staining (not shown).

172

173 ***Ototoxin treatment***

174 For neomycin treatment, a concentration of 500 µM was chosen, as it was an

175 effective concentration used by Harris et al. (2003) for minimum lateral line hair cell

176 survival, as measured by DASPEI staining. A 5 mM solution was made by adding

177 neomycin trisulfate salt hydrate (Sigma-Aldrich) to MilliQ water and used at a 1:10

178 dilution in E3 fish medium. *Tg(pou4f3:GFP)* transgenic zebrafish were treated for 60

179    minutes at 28.5°C. An equivalent volume of MilliQ water in E3 was used for the

180    control group. Zebrafish were washed three times in fresh E3 and left at 28.5°C for

181    two hours. GFP signal was screened using widefield fluorescence microscopy to

182    analyse hair cell damage. Zebrafish were fixed and stained with Alexa Fluor 647

183    phalloidin as above.

184

185    ***Fluorescence imaging***

186    For confocal imaging, fixed zebrafish embryos and larvae were mounted in 1.5% low

187    melting point (LMP) agarose in PBS, and live zebrafish were mounted in 1.5% LMP

188    agarose in E3 in WillCo glass-bottomed dishes (mounted in frontal view for 32-48

189    hpf, dorsal view for later stages). Zebrafish were imaged on a Zeiss LSM880

190    Airyscan confocal microscope equipped with a Plan-Apochromat 20×/0.8 M27 air

191    objective, LD LCI Plan-Apochromat 40×/1.2 Imm Korr DIC M27 water immersion

192    objective, or Plan-Apochromat 63×/1.4 oil DIC M27 objective. Images were acquired

193    in Airyscan SR mode, Airyscan Fast scan mode with SR sampling, or Airyscan Fast

194    scan mode with Opt sampling. Zebrafish were also imaged on a Zeiss LSM 800

195    attached to an upright microscope with a W Plan-Apochromat 40×/1.0 DIC M27 or

196    63×/1.0 M27 water dipping objective. The laser lines used were 488, 561, and 633

197    nm. Widefield imaging was performed on a Zeiss Axio Zoom.V16 fluorescence

198    stereo zoom microscope equipped with a Zeiss 60N-C 1" 1.0× C-mount and

199    AxioCam MRm camera. For fast-capture time series imaging, live zebrafish larvae

200    were mounted in 0.9% LMP agarose in E3 and imaged on a Zeiss Z1 Light-sheet

201    microscope, with 4% tricaine in E3 in the sample chamber. Imaging was performed

202    with a W Plan-Apochromat 20× objective using brightfield illumination and the 561

203    nm laser line. Images were acquired at a rate of 50.07 frames per second (fps).

204

205    ***Scanning electron microscopy***

206    For scanning electron microscopy, *ift88* homozygous mutant and phenotypically wild-

207    type sibling larvae at 4 dpf were fixed overnight in 2.5% glutaraldehyde/0.1M sodium

208    cacodylate buffer. Samples were washed in buffer, post-fixed in 2% aqueous

209    osmium tetroxide for 1 hour, washed in buffer again and then dehydrated through a

210    graded ethanol series (50%, 75%, 95%, 100%) before being dried in a mixture of

211    50% hexamethyldisilazane (HMDS) in 100% ethanol. Final drying was in 100%

212    HMDS. After removal of the final HMDS wash, samples were left to dry in a fume

213    hood overnight. Samples were mounted onto a pin stub using a Leit-C sticky tab and

214    Leit-C mounting putty, gold-coated using an Edwards S150B sputter coater, and

215    examined in a Tescan Vega3 LMU Scanning Electron Microscope at an operating

216    voltage of 15 kV and imaged using a secondary electron detector.

217

218    ***Image processing, quantification, and statistical analyses***

219    Zeiss LSM880 Airyscan confocal images were subjected to Airyscan processing on

220    Zen Black 2.3 software (Zeiss) using "Auto" Airyscan processing parameters. Further

221    processing was performed on Fiji (Schindelin et al., 2012). 3D rendering was

222    performed using the 3D Viewer plugin (Schmid et al., 2010) on Fiji. Rod projection

223    lengths were measured in 3D from confocal images using Fiji, and calculated in

224    Microsoft Excel using the PyT method (based on the Pythagorean theorem) from

225    Dummer et al. (2016). All quantifications were exported into GraphPad Prism 8,

226    which was then used for performing statistical analyses and making graphs.

227

228    Statistical analyses were carried out in GraphPad Prism 8. Datasets were

229    considered normally distributed if they passed at least one of four normality tests

230    (Anderson-Darling, D'Agostino & Pearson, Shapiro-Wilk, and Kolmogorov-Smirnov

231    tests). Statistical tests used are stated in the figure legends. Bars on graphs indicate

232    mean ± standard error of the mean (S.E.M.), unless stated otherwise. *P* values are

233    indicated as follows: $P > 0.05$ (not significant, ns), $P < 0.05$ (*), $P < 0.01$ (**), $P <$

234    $0.001$ (***), $P < 0.0001$ (****).

235

236    For mapping spatial distributions of rod cells within the olfactory pit, 2D maximum

237    intensity projection images were imported into the Desmos Graphing Calculator

238    (desmos.com). The positions and sizes of the images were adjusted to align the rims

239    of olfactory pits with an ellipse to fit the shape of the rim, defined by $\frac{(x-35)^2}{5} +$

240    $\frac{(y-33)^2}{10} = 7.6^2$. The positions of the base of each rod, relative to the ellipse, were

241    plotted as coordinates onto the graph. The resulting graphs were exported as .png

242    image files.

243

244    Figures were prepared using Adobe Photoshop.

**Results**

***Actin-rich rod-like apical projections, distinct from microvilli and cilia, are***

***present in the olfactory epithelium of larval and juvenile zebrafish***

Staining of the wild-type larval and juvenile zebrafish OE with fluorescently-
conjugated phalloidin, which binds to F-actin, reveals the presence of several actin-
rich rod-like projections ('rods') in each olfactory pit (Figure 1A-B'). These projections
differ in number, distribution, size and morphology from any of the described apical
projections of zebrafish OSNs. The projections extend from below the apical surface
of the OE and project about 10 µm above it, tapering to a point. This is an order of
magnitude longer than OSN microvilli, which are typically 0.5-0.8 µm in length
(Hansen & Zeiske, 1998). Olfactory rods are shorter than the surrounding phalloidin-
negative olfactory cilia (Fig. 1C-D'), and do not label with an anti-acetylated α-tubulin
antibody (Figure 1C-C'''). Rods are not evenly distributed across the OE, but are
mostly clustered posterolaterally in each olfactory pit, although there is variation
between individuals (Figure 1E). At low magnification, the olfactory rods appear
similar to the actin-rich stereociliary bundle of mechanosensory hair cells of the inner
ear and lateral line. However, higher magnification images reveal that the olfactory
rod is not oligovillous, but appears to be a single structure (Figure 1B', C''', D'). This
contrasts with the stepped array of multiple stereocilia present on the apical surface
of mechanosensory hair cells (Figure 1F).

To characterise the timing of appearance and development of the olfactory rods
during embryonic and larval stages, we stained fixed samples from 36 hpf, just after
formation of the olfactory pits (Hansen & Zeiske, 1993), to 5 dpf. Occasional rods
were present in olfactory pits at 36 hpf, but were only consistently present beyond 46
hpf (Figure 2A, B). Although the number of rods per olfactory pit varied at each
stage, the average number increased over time. By 5 dpf, each olfactory pit
contained 10.7 ± 2.9 (mean ± standard deviation, s.d.) rods (Figure 2B). After
measuring the rods in 3D, we found an increase in projection length (from the base
of the phalloidin-positive projection to the tip) from 36 hpf to 5 dpf, with the most
significant increase occurring by 48 hpf, despite a relatively large range in length at
each stage. At 5 dpf in fixed samples, the mean projection length was 10.4 ± 2.2
(s.d.) µm, with the largest measuring 17.5 µm (Figure 2C).

279    ***Olfactory rod cell projections can develop in the absence of olfactory cilia***

280    As described above, olfactory rods differ from olfactory cilia in terms of size, shape,

281    cytoskeletal composition, and distribution in the OE. We therefore hypothesised that

282    olfactory rod cell projections would not be affected by mutations that disrupt the

283    formation of cilia. To test this, we examined fish mutant for *ift88*, which codes for a

284    component of the intraflagellar transport machinery necessary for the normal

285    formation and maintenance of cilia (Tsujikawa & Malicki, 2004). A phalloidin stain

286    revealed that olfactory rods were present in the OE of *ift88*^{-/-} mutants at 5 dpf (Figure

287    3A, B).

288

289    The absence of cilia in *ift88*^{-/-} mutants allowed us to examine morphology of the rods

290    using scanning electron microscopy (SEM). In the phenotypically wild-type sibling

291    OE, the rods were almost completely obscured by olfactory cilia, with only the

292    occasional tip of a projection visible (Figure 3C-E''). However, SEM images of the

293    olfactory pit of *ift88*^{-/-} mutants at 4 dpf, which lack cilia, revealed the presence of rod-

294    like projections with a similar size, number, smoothly tapering morphology, and

295    spatial distribution to the actin-rich projections described above (Figure 3F-I). At their

296    base, olfactory rods are wider in diameter (about 0.6 μm) than the olfactory cilia in

297    wild-type larvae (0.2 μm in diameter, as is typical for many cilia). We conclude that

298    olfactory rods can develop in the absence of cilia.

299

300    ***Olfactory rods can be labelled in the live larva***

301    To visualise olfactory rods in live larvae, we imaged the *Tg(actb2:Lifeact-RFP)*

302    transgenic line at 4 and 6 dpf, and *Tg(actb2:Lifeact-GFP)* at 5 dpf (Behrndt et al.,

303    2012). We found fluorescent apical projections in the olfactory pits of live larvae in all

304    cases (*N* of fish = 4) (Figure 4A-C, Supplementary Movie 1). These matched the

305    size, shape, and posterolateral distribution of rod cells present in fixed samples

306    (Figure 4D, E). Despite potential shrinkage due to fixation, there was no overall

307    difference in the lengths of projections between live and fixed samples (Figure 4E).

308    The zig-zag pattern exhibited by RFP-positive olfactory rods in raster-scanned

309    images of live larvae suggested that rods were moving during image capture (Figure

310    4B). Fast-capture time series imaging of the *Tg(actb2:Lifeact-RFP)* transgenic line

311    allowed us to observe that the projection oscillates (Supplementary Movie 2),

312    possibly as a result of ciliary beating.

313

### Neuronal promoters drive reporter expression in olfactory rod cells

314 **Neuronal promoters drive reporter expression in olfactory rod cells**

315 To test whether rod cells are neuronal, we imaged two transgenic lines that have

316 broad neuronal expression of cytoplasmic fluorescent reporters –

317 *Tg(Xla.tubb:jGCaMP7f)* (Chia et al., 2019) (*N* of olfactory pits = 4) and

318 *Tg(elavl3:GCaMP6f)* (Dunn et al., 2016) (*N* = 5). Dendrites and dendritic knobs of

319 OSNs were clearly labelled by both lines. In some examples, we observed faintly-

320 labelled projections extending from the surface of the olfactory epithelium, with a

321 similar length and morphology to olfactory rods (Figure 5A-B). Imaging of double-

322 transgenic *Tg(elavl3:GCaMP6f);Tg(actb2:Lifeact-RFP)* larvae at 5 dpf indicated that

323 rods were GCaMP6f-positive (*N* of fish = 3; Figure 5C-C''). These observations

324 suggest that olfactory rod cells may be neurons.

325

### Olfactory rod cells are not hair-cell-like cells

326 **Olfactory rod cells are not hair-cell-like cells**

327 Given the superficial similarity in appearance of the olfactory rod to hair-cell

328 stereocilia in phalloidin stains, and a report of a rare cell type bearing stereocilia-like

329 microvilli in the rat OE (Menco & Jackson, 1997), we tested whether there is any

330 similarity between olfactory rod cells and mechanosensory hair cells of the inner ear

331 and lateral line. As shown in Figures 1 and 3, the zebrafish olfactory rod appears to

332 be a single structure rather than a collection of microvilli or stereocilia. To test

333 whether olfactory rod cells express sensory hair cell markers, we performed an

334 Alexa-phalloidin co-stain on the *Tg(pou4f3:GFP)* transgenic line, a known marker for

335 hair cells (Xiao et al., 2005). At 5 dpf, the stereociliary bundle of lateral line

336 neuromast hair cells was clearly marked by both GFP and phalloidin, which acted as

337 our positive control (Figure 6A-A''). However, the GFP did not co-localise with the

338 phalloidin signal in the olfactory rods, or in the cell body beneath a phalloidin-positive

339 rod (Figure 6B-B''). Additionally, confocal images of an antibody stain against

340 synaptic vesicle protein 2 (SV2), a marker of synaptic terminals of afferent neurons

341 contacting secondary sensory cells such as mechanosensory hair cells and taste

342 receptors (Buckley & Kelly, 1985; Portela-Gomes et al., 2000; Zachar & Jonz, 2012),

343 showed that SV2-positive synapses are not present in the olfactory epithelia at 4 dpf

344 (Figure 6C, D). This contrasted with strong staining of synaptic terminals in cranial

345 lateral line neuromasts in the vicinity of the olfactory pits (Fig. 6C, D).

346

347   We next investigated whether treatment with neomycin, an aminoglycoside antibiotic

348   and well-described ototoxin, has the same damaging effect on olfactory rod cells as

349   on lateral line hair cells (Harris et al., 2003). Following neomycin treatment at 500

350   μM for 60 minutes on 3 dpf *Tg(pou4f3:GFP)* larvae, lateral line hair cells were lost or

351   severely damaged, as determined by a decrease in the number of GFP-positive cells

352   in both cranial and trunk neuromasts and a change in morphology of any remaining

353   cells (Figure 6E-H). By contrast, olfactory rods appeared unaffected (Figure 6I, J),

354   with no significant change in the number of rods present in each olfactory pit (Figure

355   6K). Taken together, the smooth appearance of the olfactory rods, lack of hair cell

356   and synaptic vesicle marker expression, and resistance to neomycin indicate that

357   olfactory rod cells are not closely related to hair cells.

358

359   ***A sub-population of olfactory rod cells expresses a Lifeact transgene driven***

360   ***by the sox10 promoter***

361   Sox10 is a known marker of both neural crest and otic epithelium (Dutton et al.,

362   2001). Robust transgene expression driven by the *sox10* promoter has been

363   reported in the OE and other tissues in the zebrafish (Mongera et al., 2013; Saxena

364   et al., 2013). We have generated a *Tg(sox10:Lifeact-mRFPruby)* transgenic line to

365   visualise actin localisation and dynamics in the live embryo in *sox10*-expressing

366   tissues. As reported for the *Tg(sox10:eGFP)* transgene (Saxena et al., 2013), we

367   observed OSNs expressing *Tg(sox10:Lifeact-mRFPruby)* in the OE at 4 and 5 dpf;

368   based on morphology, most of these cells were microvillous neurons. However,

369   staining with Alexa-phalloidin on fixed samples revealed the co-expression of Lifeact-

370   mRFPruby in a sub-population of phalloidin-positive olfactory rod cell projections

371   (Figure 7A-B''). Not all olfactory rod cells expressed the transgene; an average of

372   64.4% of rod cells marked by phalloidin (*N* of olfactory pits = 5, *n* of olfactory rods =

373   59) also expressed Lifeact-mRFPruby (Figure 7C). As for the rods labelled with

374   Lifeact-RFP, rods labelled with Lifeact-mRFPruby oscillated (Supplementary Movie

375   3).

376

377   The sparse expression of the *Tg(sox10:Lifeact-mRFPruby)* transgene allowed us to

378   visualise the morphology of the cell body of olfactory rod cells and ask whether they

379   have an axon. Lifeact-mRFPruby-expressing cell bodies were positioned apically in

380   the OE and were rounded in shape (Figure 7B-B'', E). They were morphologically

381 distinct from the well-described microvillous neurons (Figure 7D, E) as well as

382 ciliated and crypt OSNs. The axons of microvillous OSNs were visible in those cells

383 labelled by the transgene (Figure 7D). However, with this marker, we were unable to

384 observe an axon extending from the cell body of olfactory rod cells (*N* of olfactory

385 pits = 5, *n* of cells = 9; Figure 7E).

386

387 To test whether the development of olfactory rod cells is dependent on *sox10*

388 function, we stained *sox10$^{-/-}$* homozygous mutants (Dutton et al., 2001) with Alexa-

389 phalloidin. Olfactory rods were present in *sox10$^{-/-}$* mutants at 5 dpf, but variable in

390 number (*N* of olfactory pits = 8, *n* of olfactory rods = 53; Figure 8). Taken together,

391 the data from *Tg(sox10:Lifeact-mRFPruby)* transgenic and *sox10$^{-/-}$* mutant larvae

392 indicate that *sox10* function is not essential for the formation of olfactory rods.

393

394    **Discussion**

395    Through the use of phalloidin staining, immunohistochemistry, transgenic zebrafish

396    lines, SEM and high-resolution fluorescence confocal imaging, we have identified a

397    rare cell type, the olfactory rod cell, in the zebrafish larval and juvenile OE. Olfactory

398    rod cells, which have not previously been described in zebrafish to our knowledge,

399    are morphologically distinct from the well-characterised OSNs and other known cell

400    types in terms of their apical projections, cell shape, and distribution and positioning

401    within the OE.

402

403    *The olfactory rod: an actin-rich apical projection*

404    The spectacular actin-rich projection of the olfactory rod cell adds to the rich

405    repertoire of known F-actin-based cellular specialisations, which include microvilli,

406    stereocilia, lamellipodia, filopodia, cytonemes and microridges (reviewed in [Heath &

407    Holifield, 1991; Theriot & Mitchison, 1991]; Ramírez-Weber & Kornberg, 1999; Pinto

408    et al., 2019; Inaba et al., 2020). Many classes of sensory cell, in both fish and

409    mammals, bear actin-rich mechano- or chemosensory microvillous projections,

410    including the stereocilia of sensory hair cells (Tilney et al., 1980; reviewed in

411    [Gillespie & Müller, 2009; Barr-Gillespie, 2015]), and the microvilli of olfactory and

412    vomeronasal microvillous neurons, solitary chemosensory cells (SCCs) of the skin

413    and barbel (Kotrschal et al., 1997; Finger et al., 2003), taste bud cells (Hansen et al.,

414    2002; Zachar & Jonz, 2012), spinal cerebrospinal fluid-contacting neurons (CSF-

415    cNs; Djenoune et al., 2014; Desban et al., 2019), Merkel cells, retinal Müller glia

416    (Sekerková et al., 2004), and the brush and tuft cells of mammalian respiratory and

417    intestinal epithelia, respectively (reviewed in [Reid et al., 2005; Schneider et al.,

418    2019]). As a single structure with a smoothly tapering morphology, the zebrafish

419    olfactory rod differs from these oligovillous structures. Adult zebrafish SCCs, found

420    distributed over the entire body surface (Kotrschal et al., 1997), and mature light

421    cells of the zebrafish taste bud (Hansen et al., 2002) each bear a single microvillus,

422    but at 1-3 µm in length, these are much shorter than the olfactory rods we describe.

423

424    A note on terminology: olfactory rod cells are distinct from rodlet cells, which have

425    been reported in many different epithelial tissues (including OE) of marine and

426    freshwater fish, including zebrafish, and contain several intracellular electron-dense

427    rodlets within a thick cuticular-like wall (Bannister, 1966; reviewed in [Morrison &

428    Odense, 1978]; Hansen & Zeiske, 1998 Dezfuli et al., 2007; DePasquale, 2020).

429    Recently, phalloidin staining has demonstrated that the rodlets, which can be

430    extruded from the cell, are not composed of F-actin (DePasquale, 2020). Thus,

431    zebrafish olfactory rod cells, which are unique to the OE at the larval stages we have

432    described, are not related to rodlet cells.

433

434    ***Olfactory rod cells in other teleost species***

435    Previous studies have provided brief descriptions of similar cell types in other teleost

436    species, including the common minnow (Bannister, 1965), several eel species

437    (Schulte, 1972; Yamamoto & Ueda, 1978), goldfish (Breipohl et al., 1973; Ichikawa &

438    Ueda, 1977), rainbow trout (Rhein et al., 1981), common bleak (Hernádi, 1993),

439    catfish (Datta & Bandopadhyay, 1997), and several cave fish and cave loach species

440    (Waryani et al., 2013; Waryani et al., 2015; Zhang et al., 2018).

441

442    Using transmission electron microscopy (TEM), Bannister (1965) reported sparsely-

443    populated rod-shaped protrusions, approximately 4 µm in length and shorter than

444    surrounding sensory and non-sensory olfactory cilia, in the OE of adult (3.7 cm)

445    common minnow (*Phoxinus phoxinus*)*.* Here, the rod-like projection consisted of

446    several bundles of fibres, consistent with the appearance of F-actin, extending from

447    deep within the cell (Bannister, 1965). Similarly, using TEM and SEM respectively,

448    Schulte (1972) and Yamamoto and Ueda (1978) reported the presence of olfactory

449    rod cells in the OE of several adult eel species: European eel (*Anguilla anguilla*),

450    Japanese eel (*A. japonica*), white-spotted conger (*Conger myriaster*), buffoon snake

451    eel (*Microdonophis erabo*), and brutal moray (*Gymnothorax kikado*). In European

452    eels, the cells were described as a receptor with a single rod-shaped appendage,

453    measuring 0.8 µm in diameter and extending 4 µm above the apical surface of the

454    epithelium (Schulte, 1972). Olfactory rods in the other four species measured 1 µm

455    in diameter and 10 µm in length. Rods were either found to exist solitarily or in a

456    group; interestingly, it was noted that olfactory cilia were sparse in areas where rods

457    occurred in a group (Yamamoto & Ueda, 1978).

458

459    More recent reports include comparisons of the surface structures of olfactory

460    epithelia in different adult cave fish and loaches. SEMs in *Sinocyclocheilus jii* and *S.*

461    *furcodorsalis* cave fish, and in *Oreonectes polystigmus* and *O. guananensis* cave

462 loaches revealed that olfactory rods were clustered in different regions of olfactory

463 rosette lamellae (Waryani et al., 2013; Waryani et al., 2015). Another SEM study on

464 the variations in olfactory systems of adult cave fish species of different habitats

465 reported not just one, but three different cell types all classified as 'rod cilia' in the

466 olfactory epithelia of *S. anshuiensis* and *S. tianlinensis*. The first cell type had a long

467 base with an oval apex, the second contained an oval base with a thin apex, while

468 the third was rod-shaped and thin from base to tip, measuring 2.01-3.08 μm in length

469 (Zhang et al., 2018). Despite the shorter length, this third type appeared

470 morphologically consistent with zebrafish olfactory rod cells. Unlike other teleosts,

471 olfactory rod cells were reported as the dominant cell type over ciliated and

472 microvillous neurons in the OE of *S. jii* (Waryani et al., 2013). This may be an

473 example of the known compensatory enhancement of the olfactory system in blind

474 morphs of cave fish (Bibliowicz et al., 2013; reviewed in [Krishnan & Rohner, 2017]).

475

476 Although there appear to be variations in the numbers and sizes of olfactory rod cells

477 reported in these other teleost species, some of these cells may be homologous to

478 the olfactory rod cells we describe in zebrafish larvae. However, all of these previous

479 studies were limited to fixed adult samples by means of TEM and SEM, and none

480 have tested or confirmed the molecular composition of the rod.

481

482 ***Olfactory rod cells differ from known olfactory sensory neurons or secondary***

483 ***receptor cells***

484 We have detected weak expression of cytoplasmic fluorescent markers driven by

485 neuronal promoters in olfactory rod cells, suggesting they are a type of OSN.

486 However, we were unable to detect an axon in nine individual olfactory rod cells

487 imaged with a Lifeact-mRFPruby transgene at 4-5 dpf. Of note, Ichikawa and Ueda

488 (1977) performed olfactory nerve bundle transection in adult goldfish to determine

489 which cell types are olfactory receptors. As expected, transection caused retrograde

490 degeneration of both ciliated and microvillous OSNs. Olfactory rod cells, however,

491 were still identifiable by SEM in the OE 10 days after nerve transection. The authors

492 concluded that adult goldfish olfactory rod cells are not sensory receptor cells;

493 however, the result could also indicate differences in regeneration kinetics between

494 different neuronal cell types.

495

496    The shape, position and actin-rich projection of zebrafish olfactory rod cells,

497    however, do have some similarities to those of kappe OSNs, identified to date only in

498    adult zebrafish OE (Ahuja et al., 2014). The actin-positive apical specialisation of

499    kappe cells differs in morphology from the rods we describe, and is thought to

500    consist of microvilli, although this has not been confirmed at an ultrastructural level.

501    Kappe neurons were reported to have an axon, and were thus interpreted as a class

502    of OSN (Ahuja et al., 2014). It will be important to determine whether olfactory rod

503    cells are present in the adult zebrafish OE and how their morphology relates to

504    kappe cells.

505

506    Olfactory rod cells do not appear to share characteristics with sensory hair cells. As

507    a monovillous structure, the olfactory rod is quite unlike the stereociliary bundle of a

508    hair cell; moreover, the cells do not express known hair cell markers, and are

509    insensitive to the aminoglycoside antibiotic neomycin, a potent ototoxin. In addition,

510    the entire olfactory pit was negative for the synaptic vesicle and neuroendocrine cell

511    marker SV2 (Buckley & Kelly, 1985; Portela-Gomes et al., 2000), indicating that

512    olfactory rod cells are unlikely to be secondary sensory cells innervated by afferent

513    neurons.

514

515    ***Olfactory rod cells as artefact***

516    Since the first report of olfactory rod cells, several studies have proposed that they

517    may represent senescent forms of OSNs or fixation artefacts (Muller & Marc, 1984;

518    Moran et al., 1992; reviewed in [Hansen & Zielinski, 2005]). A study in the goldfish

519    (*Carassius auratus*) and channel catfish (*Ictalurus punctatus*), using TEM, SEM and

520    filling with horseradish peroxidase, concluded that rods are most likely a result of

521    fusion of olfactory cilia or microvilli – an indicator of ageing OSNs (Muller & Marc,

522    1984). A later study on the ultrastructure of olfactory mucosa in brown trout (*Salmo*

523    *trutta*) also classified rods as products of the fusion of olfactory cilia during fixation

524    (Moran et al., 1992). Indeed, TEM images in this study showed multiple ciliary

525    axonemes surrounded by a single membrane (Moran et al., 1992). The presence of

526    such fixation artefacts has led to frequent dismissal of olfactory rod cells in the

527    literature, for example in juvenile and adult European eels (Sola et al., 1993). In the

528    zebrafish, however, the olfactory rods we describe are clearly not a fixation artefact,

529    as they are present in the live larva. Moreover, they are not formed by fusion of cilia,

530    as the olfactory rods are F-actin-positive, do not stain with an anti-acetylated α-

531    tubulin antibody, and are present in *ift88*^{-/-} mutants, which lack cilia.

532

### Possible functions of olfactory rod cells

534    Actin-rich projections on sensory cells are known to have mechanosensory

535    (reviewed in [Gillespie & Müller, 2009]), chemosensory (Höfer & Drenckhahn, 1999;

536    Hansen et al., 2002; Zachar & Jonz, 2012), or multimodal functions (for example in

537    CSF-cNs in zebrafish; Djenoune et al., 2014; Desban et al., 2019). A

538    mechanosensory role for zebrafish olfactory rod cells, for example in detecting ciliary

539    movement or ciliary-driven fluid flow, or a chemosensory role in detecting odorants,

540    could aid olfactory perception in the larva. The olfactory rod cell has previously been

541    referred to as a sensory receptor cell in studies of other teleost species (Bannister,

542    1965; Schulte, 1972; Breipohl et al., 1973; Waryani et al., 2013; Waryani et al.,

543    2015). Although functions were not explicitly investigated, Bannister (1965)

544    speculated that based on their internal structure, minnow olfactory rod cells perform

545    specific chemosensory roles. Another possibility is that they could correspond to

546    brush or tuft cells in air-breathing mammals, which have important roles in immunity

547    (Andres, 1975; reviewed in [Reid et al., 2005]; Howitt et al., 2016; reviewed in

548    [Schneider et al., 2019]). These ideas remain to be tested.

549

### Possible origins of olfactory rod cells

551    Our work does not address the developmental origin of olfactory rod cells, but it is of

552    interest that they express a *sox10*-driven transgene, albeit in a mosaic fashion.

553    *Sox10* mRNA is frequently described as a neural crest marker, but is also expressed

554    strongly in otic epithelium (Dutton et al., 2001), a placodally-derived tissue. The use

555    of *sox10*-driven transgenic lines to identify neural crest derivatives remains

556    controversial. Expression of a *sox10*:eGFP transgene together with photoconversion

557    studies has led to the conclusion that a subpopulation of microvillous neurons in the

558    OE is derived from neural crest (Saxena et al., 2013), and use of an inducible

559    *sox10*:ER[T2]-*Cre* transgenic line has identified previously 'contested' neural crest

560    derivatives, including cells in the sensory barbels (Mongera et al., 2013). However,

561    using lineage reconstruction through backtracking and photoconversion experiments,

562    Aguillon et al. (2018) have argued that all olfactory neurons, including OSNs and

563    gonadotropin-releasing hormone 3 (GnRH3) cells, are derived entirely from

564  preplacodal progenitors. We think it likely that olfactory rod cells are placodally-

565  derived, but this remains to be confirmed.

566

567  The *Tg(sox10:Lifeact-mFRPruby)* line is expressed in a subset of both olfactory rod

568  cells and of microvillous neurons, with variation in the proportion of expressing cells

569  between individuals. This could reflect true heterogeneity in the olfactory rod cell and

570  microvillous neuron populations, or it could be a result of mosaic or leaky expression

571  of the transgene. Mosaic expression is typical for many transgenes (Mosimann et al.,

572  2013), while leaky expression, which can be explained through the lack of

573  appropriate silencer elements (Jessen et al., 1999), is suspected for the *sox10*

574  promoter fragment used in our transgenic construct (reviewed in [Tang & Bronner,

575  2020]). Nevertheless, the *Tg(sox10:Lifeact-mRFPruby)* line has proved a fortuitous

576  tool for visualising olfactory rod cells in the live larva.

577

578  ***Concluding remarks***

579  As a key model organism for the study of the olfactory system (reviewed in [Kermen

580  et al., 2013; Calvo-Ochoa & Byrd-Jacobs, 2019]), a complete inventory of the cell

581  types present in the zebrafish OE will be an important resource and reference point

582  for further study. Olfactory dysfunction can signify underlying cellular disorders and

583  can also be implicated in neurodegenerative diseases (reviewed in [Whitlock, 2015];

584  Bergboer et al., 2018). OSNs project directly to the OB, and thus provide an entry

585  route for pathogens to the brain (reviewed in [Dando et al., 2014]). Cells in the OE

586  can themselves be damaged by viral infection, leading to a reduction, change, or

587  loss of sense of smell, a phenomenon that has attracted much recent attention due

588  to the damaging action of SARS-CoV-2 on the human olfactory system (Brann et al.,

589  2020; Gupta et al., 2020). In the zebrafish, new functions of the OE, such as the

590  detection of sodium and chloride ions (Herrera et al., 2020), continue to be

591  uncovered. Addressing the functions of the olfactory rod cell will be an important next

592  step.

593

594 **Ethics**

595 All zebrafish work in Sheffield was undertaken under licence from the UK Home

596 Office and according to recommended standard husbandry conditions (Aleström et

597 al., 2019). All experiments in Singapore were performed under guidelines approved

598 by the Institutional Animal Care and Use Committee of Biopolis.

599

600 **Conflict of Interest**

601 The authors declare no competing interests.

602

603 **Author Contributions**

604 Designed the research: KYC, TTW, SJJ. Conducted the experiments: KYC, SJJ,

605 TTW, SB, NJvH, MM, CJH. Data analysis: KYC, SJJ, TTW. Writing (original draft):

606 KYC, TTW; writing (review and editing): KYC, TTW, SJJ, with additional

607 contributions from SB, NJvH, CJH.

608

627

**Figures**

**Figure 1. Phalloidin staining reveals the presence of actin-rich rod-like projections, distinct from microvilli and cilia, in the zebrafish larval and juvenile olfactory epithelium.**
(A) Maximum intensity projection of an Airyscan confocal image of phalloidin stain in an olfactory pit of a 5 dpf wild-type larva; anterior to the top right, lateral to the bottom right. Arrowhead marks one example olfactory rod. Scale bar = 20 μm. (A') Enlargement of olfactory rods in A. Scale bar = 5 μm. (B) Dorsal view low power image of phalloidin stain in the head of an 18 dpf (5 mm) wild-type juvenile zebrafish; anterior to the top. Arrowhead marks the position of two olfactory rods in an olfactory pit. Scale bar = 50 μm. (B') Enlargement of OE in B. Arrowhead marks two olfactory rods. Scale bar = 10 μm. (C-C'') Airyscan confocal image of Alexa-phalloidin signal (C), acetylated α-tubulin immunohistochemistry signal (C'), and merged signals (C'') in an olfactory pit of a 4 dpf wild-type larva; anterior to the top, lateral to the right. Arrowhead marks one example olfactory rod. Scale bar = 20 μm. (C''') Enlargement of olfactory rod in C''. Scale bar = 5 μm. (D) Differential interference contrast (DIC) image and phalloidin stain (red) in an olfactory pit of a 5 dpf wild-type larva; anterior to the top, lateral to the right. Arrowhead marks one example olfactory rod. Scale bar = 20 μm. (D') Enlargement of olfactory rods in D. Surrounding olfactory cilia are visible and unlabelled by Alexa-phalloidin. Scale bar = 5 μm. (E) A map of the positions of olfactory rod cell projection bases in olfactory pits of 4 dpf wild-type larvae (*N* of olfactory pits = 5), based on 2D maximum intensity projections of confocal images of phalloidin stains; anterior 'A' to the top, lateral 'L' to the right. One dot represents one olfactory rod. Different coloured dots represent rods from different larvae. (F) Airyscan confocal image of phalloidin stain in an inner ear crista of a 5 dpf wild-type larva. Hair cell stereocilia are labelled with Alexa-phalloidin, and are arranged in a stepped array. In the stereociliary bundle on the extreme left, four different stereociliary lengths are visible (compare with A'). Scale bar = 5 μm.
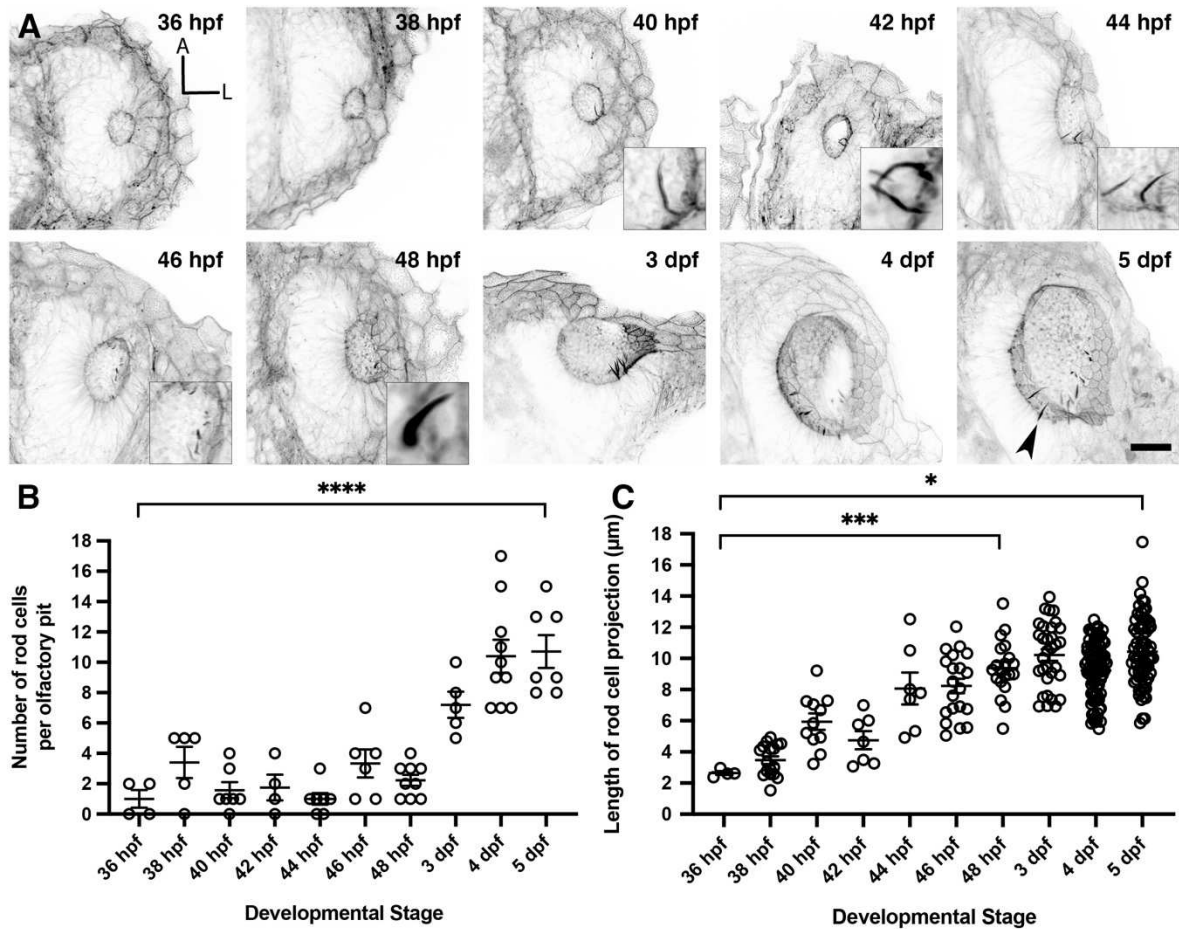
**Figure 2. Olfactory rod cells arise early during zebrafish olfactory pit development.**
(A) Maximum intensity projections of Airyscan confocal images showing the wild-type development of olfactory pit and olfactory rod cells at various embryonic and larval stages, using Alexa-phalloidin as a marker; anterior 'A' to the top, lateral 'L' to the right. Grayscale values from the original fluorescence image have been inverted. Arrowhead marks one example olfactory rod. Scale bar = 20 µm. Selected inserts show olfactory rods at higher magnification. (B) The change in number of olfactory rod cells per olfactory pit during embryonic development – 36 hpf ($N$ of olfactory pits = 4), 38 hpf ($N$ = 5), 40 hpf ($N$ = 7), 42 hpf ($N$ = 4), 44 hpf ($N$ = 7), 46 hpf ($N$ = 6), 48 hpf ($N$ = 9), 3 dpf ($N$ = 5), 4 dpf ($N$ = 10), and 5 dpf ($N$ = 7). Bars indicate mean ± S.E.M. for each stage. Linear regression analysis; **** indicates $P$ < 0.0001. (C) The change in lengths of olfactory rod cell projections during embryonic development – 36 hpf ($N$ of olfactory pits = 2, $n$ of olfactory rods = 4), 38 hpf ($N$ = 4, $n$ = 17), 40 hpf ($N$ = 6, $n$ = 11), 42 hpf ($N$ = 3, $n$ = 7), 44 hpf ($N$ = 5, $n$ = 7), 46 hpf ($N$ = 6, $n$ = 20), 48 hpf ($N$ = 9, $n$ = 20), 3 dpf ($N$ = 5, $n$ = 32), 4 dpf ($N$ = 10, $n$ = 82), and 5 dpf ($N$ = 8, 71). Bars indicate mean ± S.E.M. for each stage. Linear regression analysis; * indicates $P$ = 0.0251, *** indicates $P$ = 0.0009.
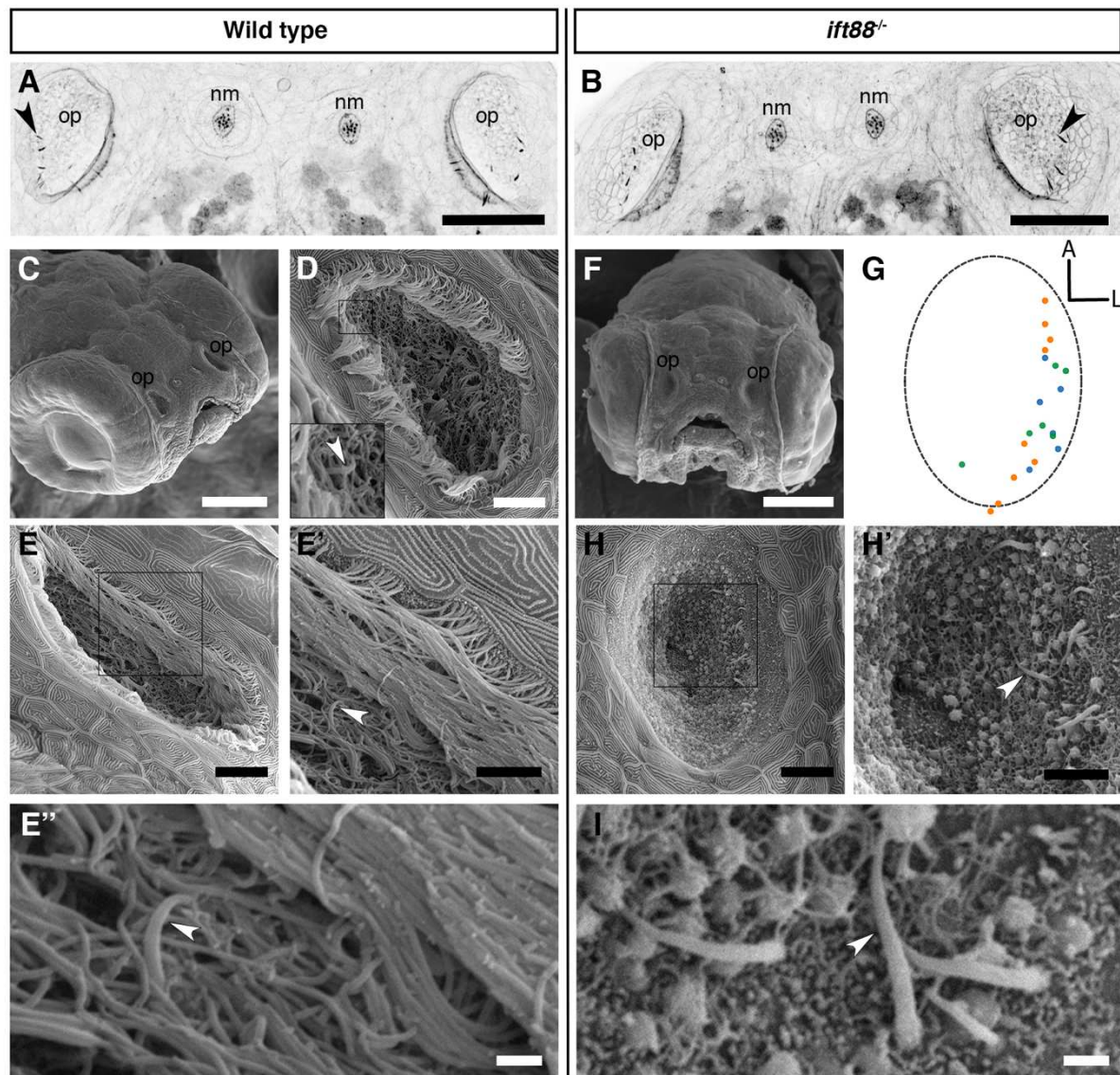
**Figure 3. Olfactory rod cells are present in the olfactory epithelia of *ift88*^{-/-} zebrafish mutants, which lack cilia.**
(A, B) Maximum intensity projections of Airyscan confocal images of phalloidin stains of a 5 dpf wild-type (A) and *ift88*^{-/-} mutant (B) larva; dorsal views, anterior to the top. Grayscale values from the original fluorescence image have been inverted. Abbreviations: nm, cranial neuromast; op, olfactory pit. Several olfactory rods (arrowheads mark examples) are visible in each olfactory pit. Scale bar = 50 μm. (C) SEM of the head of a 4 dpf wild-type larva. Scale bar = 100 μm. (D-E) SEM of 4 dpf larval wild-type olfactory pits (enlarged from panel C). Scale bars = 10 μm. Insert in D shows enlarged view of boxed area in D. Arrowhead marks the tip of a rod cell apical projection surrounded by olfactory cilia. (E') Enlarged view of boxed area in E. Arrowhead marks one olfactory rod. Scale bar = 5 μm. (E'') Enlargement of olfactory rod in E' (arrowhead). Scale bar = 1 μm. (F) Frontal view SEM of the head of a 4 dpf *ift88*^{-/-} mutant larva. Scale bar = 100 μm. (G) A map of the positions of olfactory rod cell projection emergence through the OE in *ift88*^{-/-} mutant larvae (*N* of olfactory pits = 3), based on SEM images at 4 dpf; anterior 'A' to the top, lateral 'L' to the right. One dot represents one olfactory rod. Different coloured dots represent rods from different larvae. (Compare with Figure 1E.) (H) SEM of 4 dpf larval *ift88*^{-/-} mutant olfactory pit (enlarged from panel F). Scale bar = 10 μm (H') Enlarged view of boxed area in H. Arrowhead marks one example olfactory rod cell projection present despite the loss of cilia. Scale bar = 5 μm. (I) Enlarged SEM of olfactory rods (arrowhead marks example) in 4 dpf larval *ift88*^{-/-} mutant olfactory pit (from a different individual). Scale bar = 1 μm.
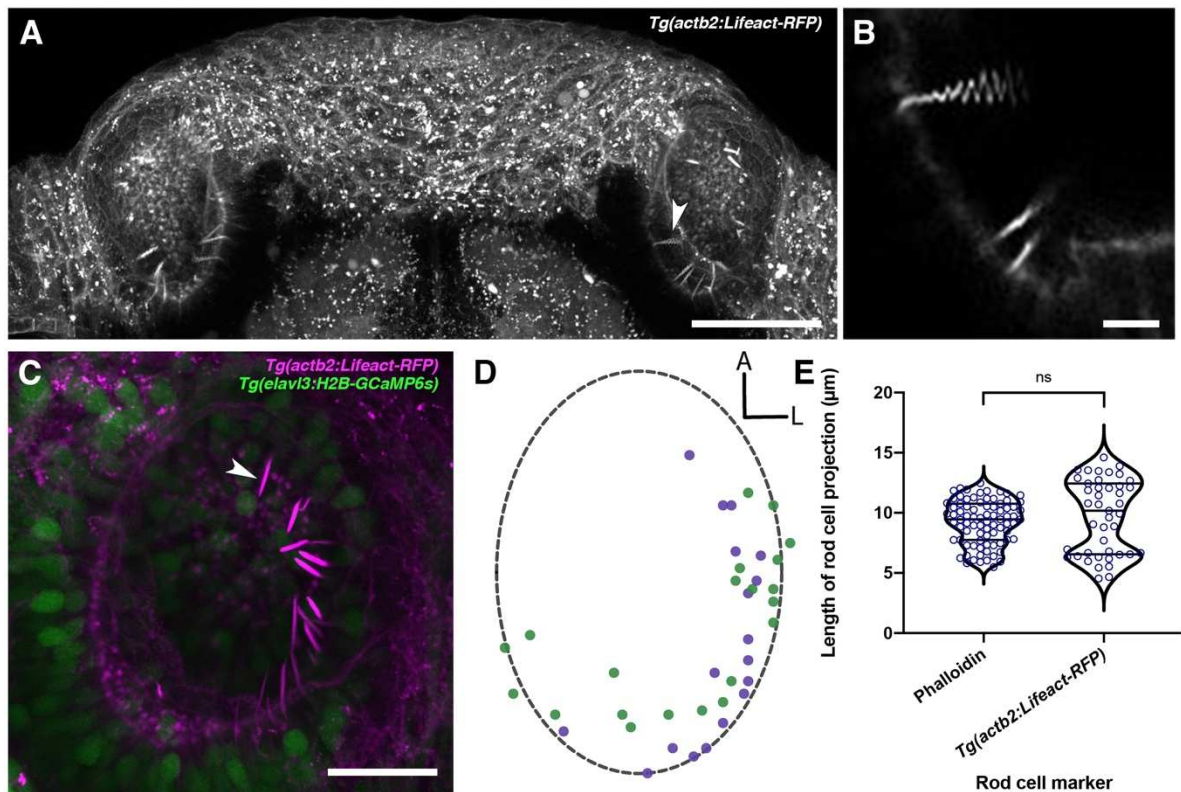
695

696

697 **Figure 4. Olfactory rods are labelled in the olfactory epithelia of live zebrafish larvae by the**
698 ***Tg(actb2:Lifeact-RFP) transgene.***
699 (A) Maximum intensity projection of dorsal view image of the olfactory pits of a live 6 dpf
700 *Tg(actb2:Lifeact-RFP)* transgenic larva; anterior to the top. Arrowhead marks one example olfactory
701 rod positive for the Lifeact-RFP transgene. Scale bar = 50 μm. (B) Enlargement of olfactory rods in A
702 (arrowhead in A) oscillating during raster-scanned image capture. (Raster scanning was performed
703 from top to bottom in the image, as it has been rotated 90° clockwise.) (See Supplementary Movie 2.)
704 Scale bar = 5 μm. (C) Maximum intensity projection image of a live 4 dpf *Tg(actb2:Lifeact-*
705 *RFP);Tg(elavl3:H2B-GCaMP6s)* double-transgenic larval olfactory pit; anterior to the top, lateral to the
706 right. Arrowhead marks one example olfactory rod positive for the Lifeact-RFP transgene (magenta).
707 Neuronal nuclei are labelled in green. Larvae were fully mounted in agarose, so rods were not
708 moving. Scale bar = 20 μm. (See Supplementary Movie 1.) (D) A map of the positions of olfactory rod
709 cell projection bases in olfactory pits of 4 dpf *Tg(actb2:Lifeact-RFP);Tg(elavl3:H2B-GCaMP6s)*
710 double-transgenic larvae (*N* of olfactory pits = 2), based on 2D maximum intensity projections of
711 confocal images; anterior 'A' to the top, lateral 'L' to the right. One dot represents one olfactory rod.
712 Different coloured dots represent rods from different larvae, with purple corresponding to panel C.
713 (Compare with Figure 1E.) (E) A quantitative comparison of the lengths of olfactory rod cell
714 projections in fixed larvae, using Alexa-phalloidin as a marker (*N* = 10, *n* of olfactory rods = 82) versus
715 live larvae, using Lifeact-RFP as a marker (*N* = 2, *n* = 43). Violin plot; bars indicate the median and
716 lower and upper quartiles for each group. Mann-Whitney U test; ns, not significant (*P* = 0.232).
717
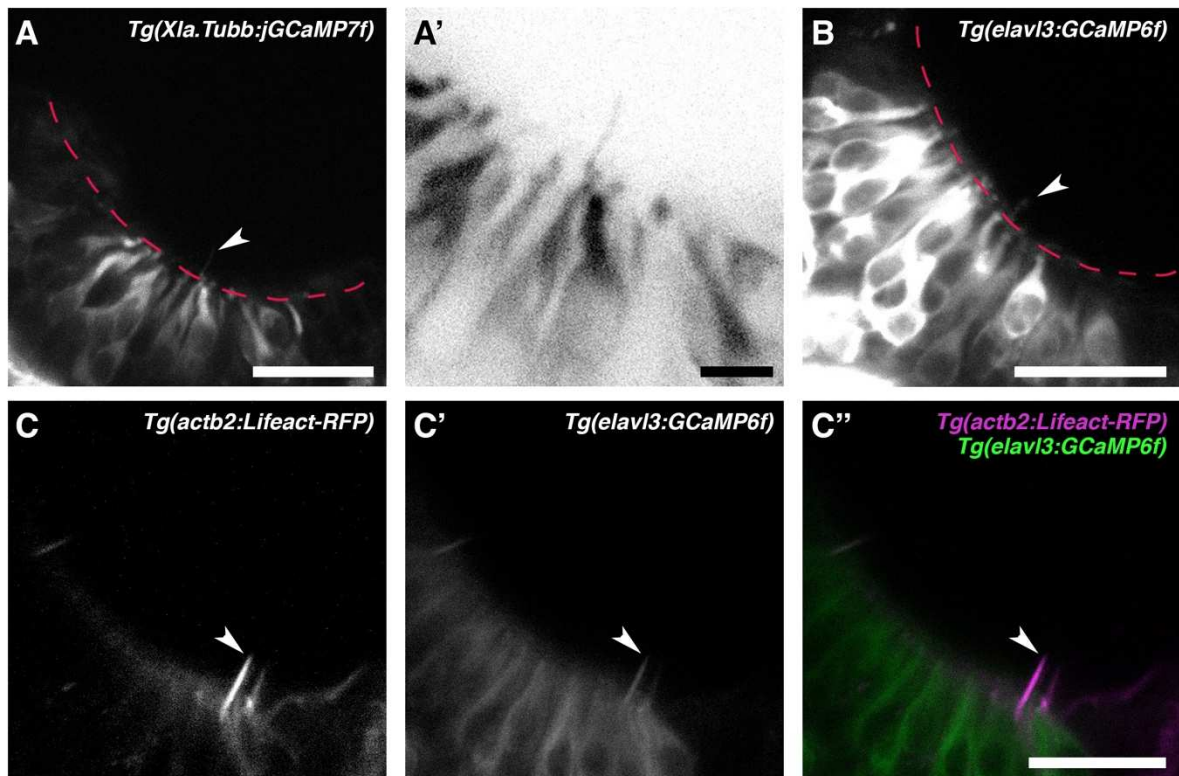
718

719

720 **Figure 5. Olfactory rod cells are labelled by the cytoplasmic neuronal markers**
721 ***Tg(Xla.Tubb:jGCaMP7f)* and *Tg(elavl3:GCaMP6f)*.**
722 (A) Olfactory pit of a 4 dpf *Tg(Xla.Tubb:jGCaMP7f)* larva; anterior to the top, lateral to the right. Red
723 dotted line outlines the apical surface of the OE; arrowhead marks one olfactory rod, albeit faintly
724 labelled. Scale bar = 20 µm. (A') Enlargement of olfactory rod marked by arrowhead in A (grayscale
725 values inverted). Scale bar = 5 µm. (B) Olfactory pit of a 5 dpf *Tg(elavl3:GCaMP6f)* larva; anterior to
726 the top, lateral to the right. Red dotted line outlines the apical surface of the OE; arrowhead marks
727 one example olfactory rod, albeit faintly labelled. Scale bar = 20 µm. (C-C'') Lifeact-RFP signal (C),
728 GCaMP6f signal (C'), and merged signals (C'') in an olfactory pit of a 5 dpf
729 *Tg(elavl3:GCaMP6f);Tg(actb2:Lifeact-RFP)* double-transgenic larva; anterior to the top, lateral to the
730 right. Arrowhead marks one example olfactory rod, positive for both Lifeact-RFP and GCaMP6f. Scale
731 bar = 20 µm.
732
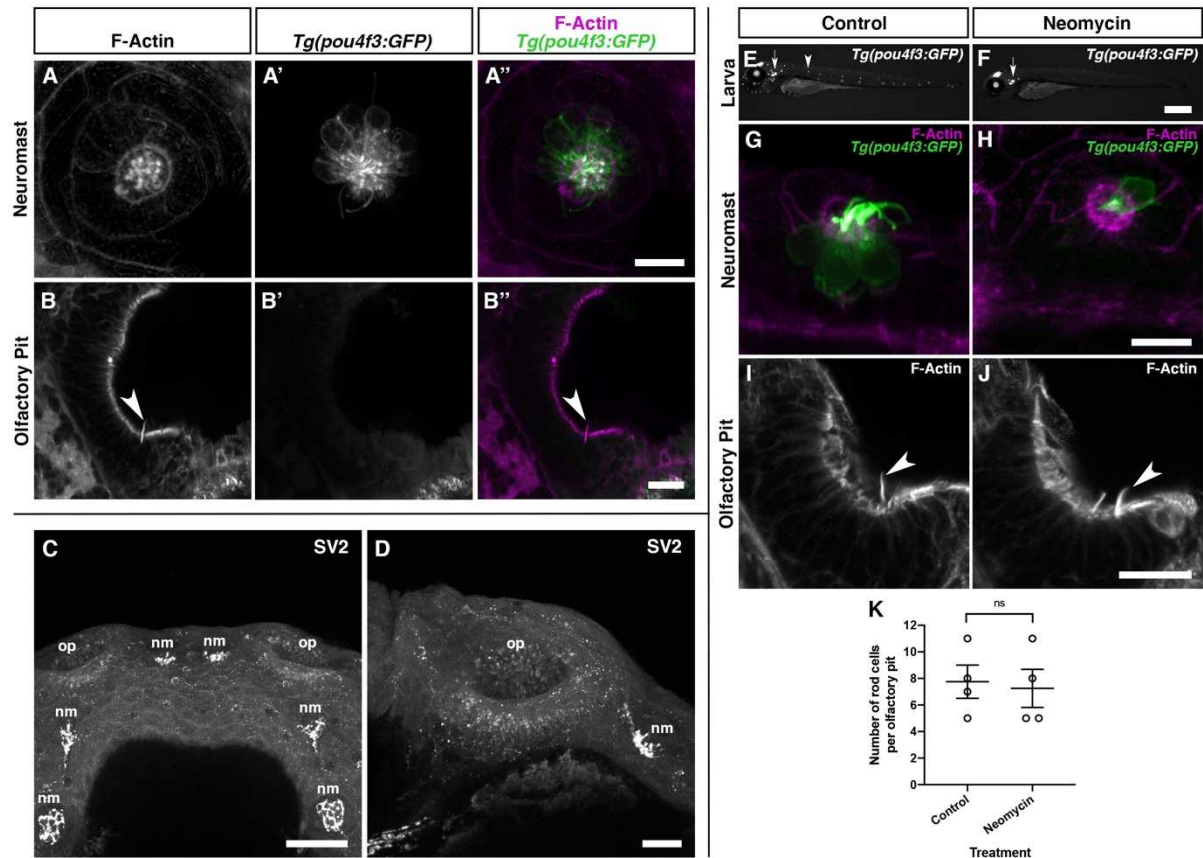
733

734

735 **Figure 6. Olfactory rod cells in the zebrafish olfactory epithelium are not hair-cell-like.**
736 (A-A'') Maximum intensity projection of Airyscan confocal image of Alexa-phalloidin signal (A),
737 *Tg(pou4f3:GFP)* signal (A'), and merged signals (A'') in a cranial neuromast of a 5 dpf larva. Scale bar
738 = 10 μm. (B-B'') Airyscan confocal image of Alexa-phalloidin signal (B), *Tg(pou4f3:GFP)* signal (B'),
739 and merged signals (B'') in an olfactory pit of a 5 dpf larva; anterior to the top, lateral to the right.
740 Arrowhead marks one olfactory rod. Scale bar = 20 μm. (C-D) Maximum intensity projections of
741 confocal images of synaptic vesicle 2 (SV2) protein immunohistochemistry signal in the heads of 4 dpf
742 wild-type larvae. Abbreviations: nm, cranial neuromast; op, olfactory pit. (C) Anterior to the top. Scale
743 bar = 50 μm. (D) Anterior to the top, lateral to the right. Scale bar = 20 μm. (E-F) Widefield imaging of
744 3 dpf *Tg(pou4f3:GFP)* larvae showing the damaging effects of 500 μM neomycin treatment for 60
745 minutes on lateral line neuromast hair cells. Fluorescence is lost or greatly reduced in both trunk
746 (arrowhead) and cranial neuromasts, whereas fluorescence in hair cells of the inner ear maculae and
747 cristae (arrow) is unaffected. Scale bar = 500 μm. (G-H) Maximum intensity projections of Airyscan
748 confocal images showing the damaging effects of 500 μM neomycin treatment for 60 minutes on hair
749 cells in a cranial neuromast of a 3 dpf larva, using *Tg(pou4f3:GFP)* (green) and Alexa-phalloidin
750 (magenta) as markers. Scale bar = 10 μm. (I-J) Maximum intensity projections of Airyscan confocal
751 images showing no effect of 500 μM neomycin treatment for 60 minutes on olfactory rods, using
752 Alexa-phalloidin as a marker; anterior to the top, lateral to the right. Arrowheads mark olfactory rods.
753 Scale bar = 20 μm. (K) The number of olfactory rod cell projections per olfactory pit of 3 dpf
754 *Tg(pou4f3:GFP)* larvae after 500 μM neomycin treatment for 60 minutes (*N* of olfactory pits = 4),
755 compared with an untreated group (*N* = 4). Welch's unpaired two-tailed *t*-test; ns, not significant (*P* =
756 0.8018).
757
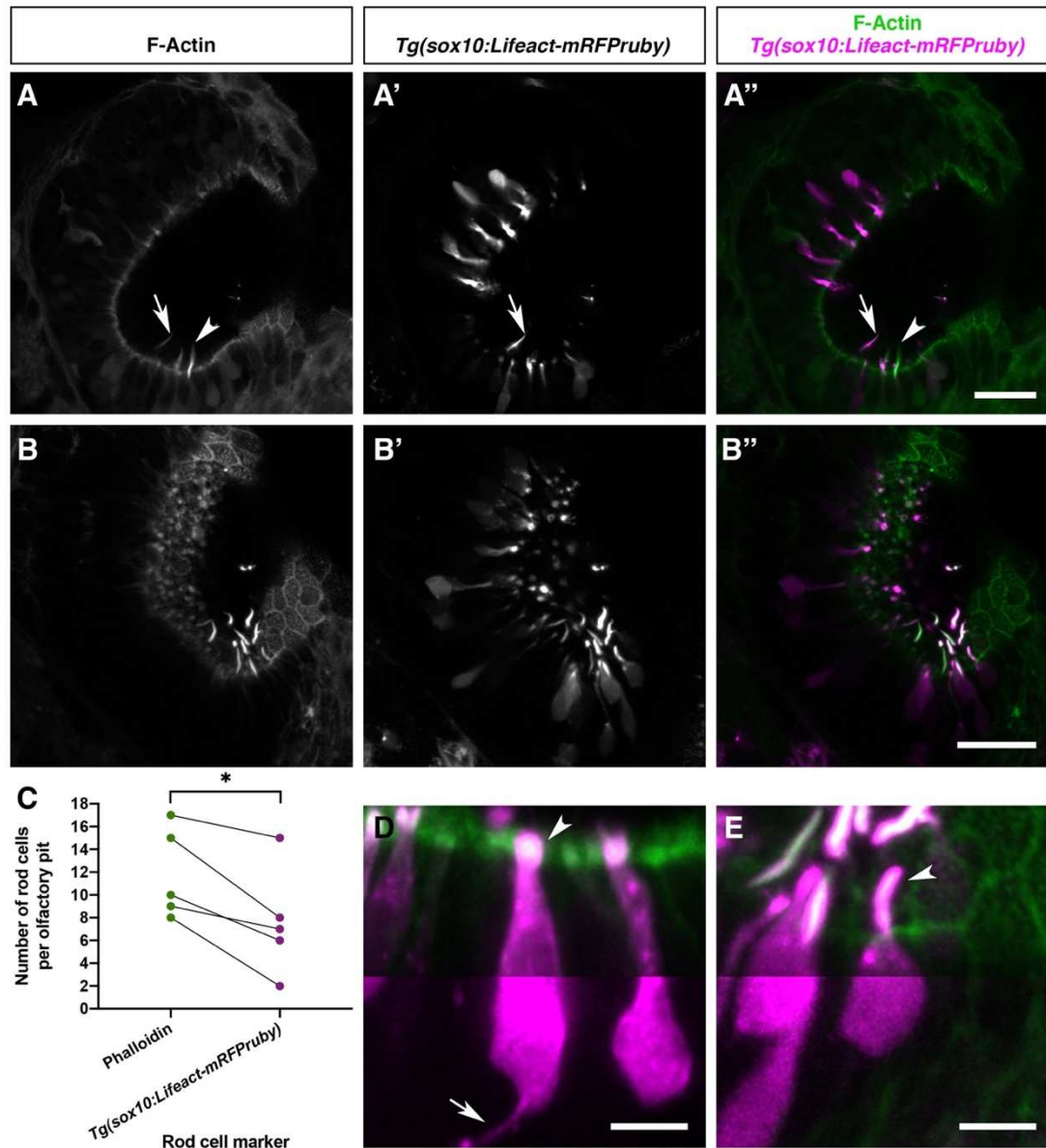
**Figure 7. Olfactory rod cells are apically located in the zebrafish olfactory epithelium, with a rounded cell body and no detectable axon.**

(A-B'') Airyscan confocal image of Alexa-phalloidin signal (A, B), *Tg(sox10:Lifeact-mRFPruby)* signal (A', B'), and merged signals (A'', B'') in olfactory pits of 4-5 dpf larvae; anterior to the top, lateral to the right. Arrowhead marks one olfactory rod negative for Lifeact-mRFPruby. Arrow marks one olfactory rod positive for Lifeact-mRFPruby. Scale bars = 20 μm. (C) Number of olfactory rod cells positively marked by Alexa-phalloidin (*n* of olfactory rods = 59), compared with the number of those also marked by *Tg(sox10:Lifeact-mRFPruby)* (*n* = 38), in olfactory pits of 4-5 dpf larvae (*N* of olfactory pits = 5). Connecting lines indicate rods from the same olfactory pit. Paired two-tailed *t*-test; * indicates *P* = 0.0146. (D) Enlargement of two microvillous OSNs, expressing Lifeact-mRFPruby, in the OE of a 4 dpf larva; Alexa-phalloidin signal (green), *Tg(sox10:Lifeact-mRFPruby)* signal (magenta). Arrowhead marks the microvillous apical projections. The gamma value for the magenta channel in the bottom half of the panel has been adjusted to show the axon from one of the cells (arrow). Scale bar = 5 μm. (E) Enlargement of olfactory rod cells (of which both the apical actin projections and cell bodies are labelled by the *Tg(sox10:Lifeact-mRFPruby)* transgene) in the OE of a 4 dpf larva; Alexa-phalloidin signal (green), *Tg(sox10:Lifeact-mRFPruby)* signal (magenta). Arrowhead marks a rod cell apical projection, positive for both markers. The gamma value for the bottom half of the panel has been adjusted as in D; no axon is visible. Scale bar = 5 μm. See also Supplementary Movie 3.

778



779

780
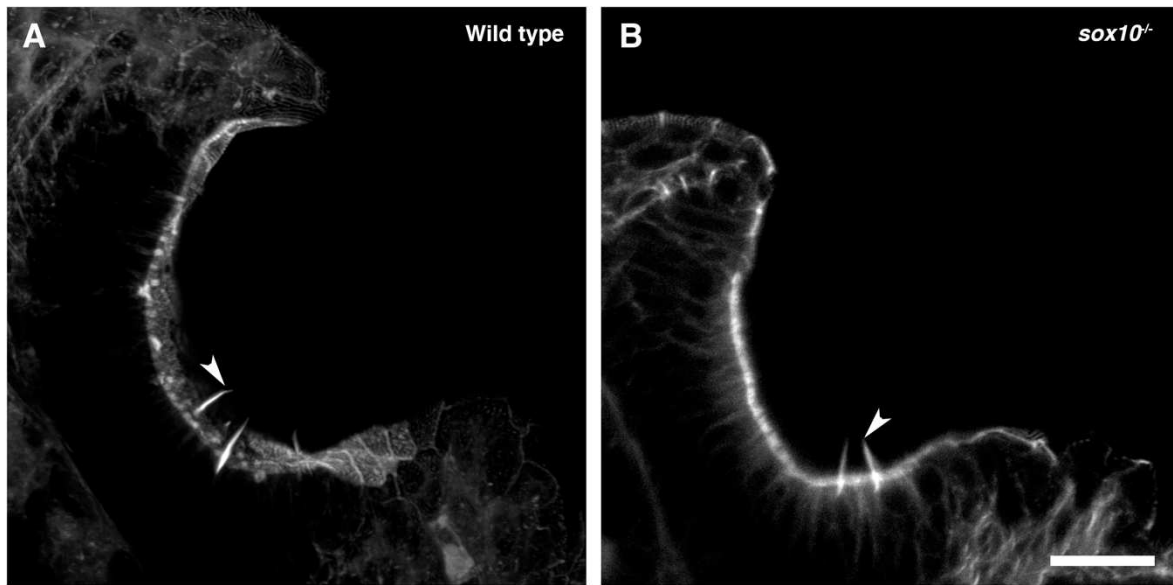
**Figure 8. Olfactory rod cells are present in the olfactory epithelia of *sox10*^{-/-} zebrafish mutants.**
(A) Maximum intensity projection of Airyscan confocal image of phalloidin stain in a 5 dpf larval wild-type olfactory pit; anterior to the top, lateral to the right. Arrowhead marks one example olfactory rod. Scale bar = 20 μm. (B) Airyscan confocal image of phalloidin stain in a 5 dpf larval *sox10*^{-/-} mutant olfactory pit; anterior to the top, lateral to the right. Arrowhead marks one example olfactory rod. Scale bar = 20 μm.

787

788 **Supplementary Material**

789

790 **Supplementary Movie 1. Olfactory rods are labelled in the olfactory epithelia of**

791 **live zebrafish by the *Tg(actb2:Lifeact-RFP)* transgene.**

792 3D rendering of a confocal image of a 4 dpf *Tg(actb2:Lifeact-RFP)*;*Tg(elavl3:H2B-*

793 *GCaMPs)* double-transgenic larval olfactory pit; anterior to the top. Olfactory rods are

794 labelled in magenta; neuronal nuclei are labelled in green.

795

796 **Supplementary Movie 2. Olfactory rods labelled with Lifeact-RFP in the**

797 **olfactory epithelia of live zebrafish larvae oscillate.**

798 Fast-capture time series confocal imaging (4.35 fps) of olfactory rods in a 6 dpf

799 *Tg(actb2:Lifeact-RFP)* larva; anterior to the top, lateral to the right. Playback speed

800 of the movie is 4 fps. Scale bar = 20 µm.

801

802 **Supplementary Movie 3. Olfactory rods labelled with Lifeact-mRFPruby in the**

803 **olfactory epithelia of live zebrafish larvae oscillate.**

804 Fast-capture time series light-sheet imaging (50.04 fps) of a 5 dpf *Tg(sox10:Lifeact-*

805 *mRFPruby)* larval olfactory pit; anterior to the top left, lateral to the top right. Beating

806 olfactory cilia are visible in brightfield (grayscale), and oscillating olfactory rods are

807 labelled by Lifeact-mRFPruby (magenta). Playback speed of the movie is 7 fps.

808 Scale bar = 20 µm.

809

810 **References**

811

812 Aguillon, R., Batut, J., Subramanian, A., Madelaine, R., Dufourcq, P., Schilling, T. F.

813     & Blader, P. (2018). Cell-Type Heterogeneity in the Early Zebrafish Olfactory

814     Epithelium Is Generated from Progenitors within Preplacodal Ectoderm. *eLife*, 7,

815     e32041.

816 Ahuja, G., Nia, S. B., Zapilko, V., Shiriagin, V., Kowatschew, D., Oka, Y. &

817     Korsching, S. I. (2014). Kappe Neurons, a Novel Population of Olfactory

818     Sensory Neurons. *Scientific Reports*, 4, 4037.

819 Aleström, P., D'Angelo, L., Midtlyng, P. J., Schorderet, D. F., Schulte-Merker, S.,

820     Sohm, F. & Warner, S. (2019). Zebrafish: Housing and Husbandry

821     Recommendations. *Laboratory Animals*, 0(0), 1–12.

822 Andres, K. H. (1975). Neue Morphologische Grundlagen Zur Physiologie Des

823     Riechens Und Schmeckens. *Archives of Oto-Rhino-Laryngology*, 210(1), 1–41.

824 Axel, R. (1995). The Molecular Logic Of Smell. *Scientific American*, 273(4), 154–159.

825 Bannister, L. H. (1965). The Fine Structure of the Olfactory Surface of Teleostean

826     Fishes. *The Quarterly Journal of Microscopical Science*, 106(4), 333–342.

827 Bannister, L. H. (1966). Is Rhabdospora Thelohani (Laguesse) a Sporozoan Parasite

828     or a Tissue Cell of Lower Vertebrates? *Parasitology*, 56(4), 633–638.

829 Barr-Gillespie, P.-G. (2015). Assembly of Hair Bundles, an Amazing Problem for Cell

830     Biology. *Molecular Biology of the Cell*, 26(15), 2727–2732.

831 Behrndt, M., Salbreux, G., Campinho, P., Hauschild, R., Oswald, F., Roensch, J.,

832     Grill, S. W. & Heisenberg, C.-P. (2012). Forces Driving Epithelial Spreading in

833     Zebrafish Gastrulation. *Science*, 338(6104), 257–260.

834 Bergboer, J. G. M., Wyatt, C., Austin-Tse, C., Yaksi, E. & Drummond, I. A. (2018).

835     Assaying Sensory Ciliopathies Using Calcium Biosensor Expression in

836     Zebrafish Ciliated Olfactory Neurons. *Cilia*, 7, 2.

837 Bettini, S., Milani, L., Lazzari, M., Maurizii, M. G. & Franceschini, V. (2017). Crypt

838     Cell Markers in the Olfactory Organ of Poecilia Reticulata: Analysis and

839     Comparison with the Fish Model Danio Rerio. *Brain Structure and Function*,

840     222(7), 3063–3074.

841 Bibliowicz, J., Alié, A., Espinasa, L., Yoshizawa, M., Blin, M., Hinaux, H., Legendre,

842     L., Père, S. & Rétaux, S. (2013). Differences in Chemosensory Response

843     between Eyed and Eyeless Astyanax Mexicanus of the Rio Subterráneo Cave.

844       *EvoDevo*, 4, 25.

845    Biechl, D., Tietje, K., Gerlach, G. & Wullimann, M. F. (2016). Crypt Cells Are

846       Involved in Kin Recognition in Larval Zebrafish. *Scientific Reports*, 6, 24590.

847    Brann, D. H. et al. (2020). Non-Neuronal Expression of SARS-CoV-2 Entry Genes in

848       the Olfactory System Suggests Mechanisms Underlying COVID-19-Associated

849       Anosmia. *Science Advances*, 6(31), eabc5801.

850    Breipohl, W., Bijvank, G. J. & Zippel, H. P. (1973). Rastermikroskopische

851       Untersuchungen Der Olfaktorischen Rezeptoren Im Riechepithel Des

852       Goldfisches (Carassius Auratus). *Zeitschrift für Zellforschung und*

853       *Mikroskopische Anatomie*, 138, 439–454.

854    Buckley, K. & Kelly, R. B. (1985). Identification of a Transmembrane Glycoprotein

855       Specific for Secretory Vesicles of Neural and Endocrine Cells. *Journal of Cell*

856       *Biology*, 100(4), 1284–1294.

857    Calvo-Ochoa, E. & Byrd-Jacobs, C. A. (2019). The Olfactory System of Zebrafish as

858       a Model for the Study of Neurotoxicity and Injury: Implications for Neuroplasticity

859       and Disease. *International Journal of Molecular Sciences*, 20(7), 1639.

860    Chia, J. S. M., Wall, E. S., Wee, C. L., Rowland, T. A. J., Cheng, R.-K., Cheow, K.,

861       Guillemin, K. & Jesuthasan, S. (2019). Bacteria Evoke Alarm Behaviour in

862       Zebrafish. *Nature Communications*, 10, 3831.

863    Dando, S. J., Mackay-Sim, A., Norton, R., Currie, B. J., St. John, J. A., Ekberg, J. A.

864       K., Batzloff, M., Ulett, G. C. & Beacham, I. R. (2014). Pathogens Penetrating the

865       Central Nervous System: Infection Pathways and the Cellular and Molecular

866       Mechanisms of Invasion. *Clinical Microbiology Reviews*, 27(4), 691–726.

867    Datta, N. C. & Bandopadhyay, S. K. (1997). Ultrastructure of Cell Types of the

868       Olfactory Epithelium in a Catfish, Heteropneustes Fossilis (Bloch). *Journal of*

869       *Biosciences*, 22(2), 233–245.

870    Demirler, M. C., Sakizli, U., Bali, B., Kocagöz, Y., Eski, S. E., Ergönen, A., Alkiraz, A.

871       S., Bayramli, X., Hassenklöver, T., Manzini, I. & Fuss, S. H. (2019). Purinergic

872       Signalling Selectively Modulates Maintenance but Not Repair Neurogenesis in

873       the Zebrafish Olfactory Epithelium. *The FEBS Journal*, 287(13), 2699–2722.

874    DePasquale, J. A. (2020). Tropomyosin and Alpha-Actinin in Teleost Rodlet Cells.

875       *Acta Zoologica*, 00, 1–10.

876    Desban, L., Prendergast, A., Roussel, J., Rosello, M., Geny, D., Wyart, C. & Bardet,

877       P.-L. (2019). Regulation of the Apical Extension Morphogenesis Tunes the

878      Mechanosensory Response of Microvilliated Neurons. *PLoS Biology*, 17(4),

879      e3000235.

880  Dezfuli, B. S., Capuano, S., Simoni, E., Previati, M. & Giari, L. (2007). Rodlet Cells

881      and the Sensory Systems in Zebrafish (Danio Rerio). *Anatomical Record*,

882      290(4), 367–374.

883  Djenoune, L., Khabou, H., Joubert, F., Quan, F. B., Figueiredo, S. N., Bodineau, L.,

884      Del Bene, F., Burcklé, C., Tostivint, H. & Wyart, C. (2014). Investigation of

885      Spinal Cerebrospinal Fluid-Contacting Neurons Expressing PKD2L1: Evidence

886      for a Conserved System from Fish to Primates. *Frontiers in Neuroanatomy*, 8,

887      26.

888  Dummer, A., Poelma, C., DeRuiter, M. C., Goumans, M.-J. T. H. & Hierck, B. P.

889      (2016). Measuring the Primary Cilium Length: Improved Method for Unbiased

890      High-Throughput Analysis. *Cilia*, 5, 7.

891  Dunn, T. W., Mu, Y., Narayan, S., Randlett, O., Naumann, E. A., Yang, C.-T., Schier,

892      A. F., Freeman, J., Engert, F. & Ahrens, M. B. (2016). Brain-Wide Mapping of

893      Neural Activity Controlling Zebrafish Exploratory Locomotion. *eLife*, 5, e12741.

894  Dutton, J. R., Antonellis, A., Carney, T. J., Rodrigues, F. S. L. M., Pavan, W. J.,

895      Ward, A. & Kelsh, R. N. (2008). An Evolutionarily Conserved Intronic Region

896      Controls the Spatiotemporal Expression of the Transcription Factor Sox10. *BMC*

897      *Developmental Biology*, 8, 105.

898  Dutton, K. A., Pauliny, A., Lopes, S. S., Elworthy, S., Carney, T. J., Rauch, J.,

899      Geisler, R., Haffter, P. & Kelsh, R. N. (2001). Zebrafish Colourless Encodes

900      Sox10 and Specifies Non-Ectomesenchymal Neural Crest Fates. *Development*,

901      128(21), 4113–4125.

902  Farnsworth, D. R., Saunders, L. M. & Miller, A. C. (2020). A Single-Cell

903      Transcriptome Atlas for Zebrafish Development. *Developmental Biology*, 459(2),

904      100–108.

905  Finger, T. E., Böttger, B., Hansen, A., Anderson, K. T., Alimohammadi, H. & Silver,

906      W. L. (2003). Solitary Chemoreceptor Cells in the Nasal Cavity Serve as

907      Sentinels of Respiration. *Proceedings of the National Academy of Sciences of*

908      *the United States of America*, 100(15), 8981–8986.

909  Galanternik, M. V., Castranova, D., Gore, A. V., Blewett, N. H., Jung, H. M.,

910      Stratman, A. N., Kirby, M. R., Iben, J., Miller, M. F., Kawakami, K., Maraia, R. J.

911      & Weinstein, B. M. (2017). A Novel Perivascular Cell Population in the Zebrafish

912      Brain. *eLife*, 6, e24369.

913    Gillespie, P. G. & Müller, U. (2009). Mechanotransduction by Hair Cells: Models,

914      Molecules, and Mechanisms. *Cell*, 139(1), 33–44.

915    Grosmaitre, X., Santarelli, L. C., Tan, J., Luo, M. & Ma, M. (2007). Dual Functions of

916      Mammalian Olfactory Sensory Neurons as Odor Detectors and Mechanical

917      Sensors. *Nature Neuroscience*, 10(3), 348–354.

918    Gupta, K., Mohanty, S. K., Mittal, A., Kalra, S., Kumar, S., Mishra, T., Ahuja, J.,

919      Sengupta, D. & Ahuja, G. (2020). The Cellular Basis of Loss of Smell in 2019-

920      NCoV-Infected Individuals. *Briefings in Bioinformatics*, 00(00), 1–9.

921    Hansen, A., Reutter, K. & Zeiske, E. (2002). Taste Bud Development in the

922      Zebrafish, Danio Rerio. *Developmental Dynamics*, 223(4), 483–496.

923    Hansen, A. & Zeiske, E. (1993). Development of the Olfactory Organ in the

924      Zebrafish, Brachydanio Rerio. *Journal of Comparative Neurology*, 333(2), 289–

925      300.

926    Hansen, A. & Zeiske, E. (1998). The Peripheral Olfactory Organ of the Zebrafish,

927      Danio Rerio: An Ultrastructural Study. *Chemical Senses*, 23(1), 39–48.

928    Hansen, A. & Zielinski, B. S. (2005). Diversity in the Olfactory Epithelium of Bony

929      Fishes: Development, Lamellar Arrangement, Sensory Neuron Cell Types and

930      Transduction Components. *Journal of Neurocytology*, 34, 183–208.

931    Harris, J. A., Cheng, A. G., Cunningham, L. L., MacDonald, G., Raible, D. W. &

932      Rubel, E. W. (2003). Neomycin-Induced Hair Cell Death and Rapid

933      Regeneration in the Lateral Line of Zebrafish (Danio Rerio). *JARO - Journal of*

934      *the Association for Research in Otolaryngology*, 4(2), 219–234.

935    Heath, J. & Holifield, B. (1991). Actin Alone in Lamellipodia. *Nature*, 352(6331), 107–

936      108.

937    Hernádi, L. (1993). Fine Structural Characterization of the Olfactory Epithelium and

938      Its Response to Divalent Cations Cd2+ in the Fish Alburnus Alburnus (Teleostei,

939      Cyprinidae): A Scanning and Transmission Electron Microscopic Study.

940      *Neurobiology*, 1(1), 11–31.

941    Hernández, P. P., Strzelecka, P. M., Athanasiadis, E. I., Hall, D., Robalo, A. F.,

942      Collins, C. M., Boudinot, P., Levraud, J.-P. & Cvejic, A. (2018). Single-Cell

943      Transcriptional Analysis Reveals ILC-like Cells in Zebrafish. *Science*

944      *Immunology*, 3(29), eaau5265.

945    Herrera, K. J., Panier, T., Guggiana-Nilo, D. & Engert, F. (2020). *Larval Zebrafish*

946    *Use Olfactory Detection of Sodium and Chloride to Avoid Salt-Water*.

947    Höfer, D. & Drenckhahn, D. (1999). Localisation of Actin, Villin, Fimbrin, Ezrin and

948    Ankyrin in Rat Taste Receptor Cells. *Histochemistry and Cell Biology*, 112(1),

949    79–86.

950    Howitt, M. R., Lavoie, S., Michaud, M., Blum, A. M., Tran, S. V., Weinstock, J. V.,

951    Gallini, C. A., Redding, K., Margolskee, R. F., Osborne, L. C., Artis, D. & Garrett,

952    W. S. (2016). Tuft Cells, Taste-Chemosensory Cells, Orchestrate Parasite Type

953    2 Immunity in the Gut. *Science*, 351(6279), 1329–1333.

954    Ichikawa, M. & Ueda, K. (1977). Fine Structure of the Olfactory Epithelium in the

955    Goldfish, Carassius Auratus. *Cell and Tissue Research*, 183(4), 445–455.

956    Inaba, Y., Chauhan, V., van Loon, A. P., Choudhury, L. S. & Sagasti, A. (2020).

957    Keratins and Plakin Family Cytolinker Proteins Control the Length of Epithelial

958    Microridge Protrusions. *eLife*, 9, e58149.

959    Iwata, R., Kiyonari, H. & Imai, T. (2017). Mechanosensory-Based Phase Coding of

960    Odor Identity in the Olfactory Bulb. *Neuron*, 96(5), 1139–1152.

961    Jessen, J. R., Willett, C. E. & Lin, S. (1999). Artificial Chromosome Transgenesis

962    Reveals Long-Distance Negative Regulation of Rag1 in Zebrafish. *Nature*

963    *Genetics*, 23, 15–16.

964    Junker, J. P., Noël, E. S., Guryev, V., Peterson, K. A., Shah, G., Huisken, J.,

965    McMahon, A. P., Berezikov, E., Bakkers, J. & Van Oudenaarden, A. (2014).

966    Genome-Wide RNA Tomography in the Zebrafish Embryo. *Cell*, 159(3), 662–

967    675.

968    Kawakami, K. (2007). Tol2: A Versatile Gene Transfer Vector in Vertebrates.

969    *Genome Biology*, 8(Suppl 1), S7.

970    Kawakami, K., Abe, G., Asada, T., Asakawa, K., Fukuda, R., Ito, A., Lal, P., Mouri,

971    N., Muto, A., Suster, M. L., Takakubo, H., Urasaki, A., Wada, H. & Yoshida, M.

972    (2010). ZTrap: Zebrafish Gene Trap and Enhancer Trap Database. *BMC*

973    *Developmental Biology*, 10, 105.

974    Kermen, F., Franco, L. M., Wyatt, C. & Yaksi, E. (2013). Neural Circuits Mediating

975    Olfactory-Driven Behavior in Fish. *Frontiers in Neural Circuits*, 7, 62.

976    Kimmel, C. B., Ballard, W. W., Kimmel, S. R., Ullmann, B. & Schilling, T. F. (1995).

977    Stages of Embryonic Development of the Zebrafish. *Developmental Dynamics*,

978    203(3), 253–310.

979    Kotrschal, K., Krautgartner, W.-D. & Hansen, A. (1997). Ontogeny of the Solitary

980    Chemosensory Cells in the Zebrafish, Danio Rerio. *Chemical Senses*, 22(2),
981    111–118.

982  Krishnan, J. & Rohner, N. (2017). Cavefish and the Basis for Eye Loss. *Philosophical
983    Transactions of the Royal Society B: Biological Sciences*, 372, 20150487.

984  Kwan, K. M., Fujimoto, E., Grabher, C., Mangum, B. D., Hardy, M. E., Campbell, D.
985    S., Parant, J. M., Yost, H. J., Kanki, J. P. & Chien, C.-B. (2007). The Tol2kit: A
986    Multisite Gateway-Based Construction Kit for Tol2 Transposon Transgenesis
987    Constructs. *Developmental Dynamics*, 236(11), 3088–3099.

988  van Lessen, M., Shibata-Germanos, S., van Impel, A., Hawkins, T. A., Rihel, J. &
989    Schulte-Merker, S. (2017). Intracellular Uptake of Macromolecules by Brain
990    Lymphatic Endothelial Cells during Zebrafish Embryonic Development. *eLife*, 6,
991    e25932.

992  Maier, E. C., Saxena, A., Alsina, B., Bronner, M. E. & Whitfield, T. T. (2014).
993    Sensational Placodes: Neurogenesis in the Otic and Olfactory Systems.
994    *Developmental Biology*, 389(1), 50–67.

995  Menco, B. P. M. & Jackson, J. E. (1997). Cells Resembling Hair Cells in Developing
996    Rat Olfactory and Nasal Respiratory Epithelia. *Tissue and Cell*, 29(6), 707–713.

997  Mongera, A., Singh, A. P., Levesque, M. P., Chen, Y. Y., Konstantinidis, P. &
998    Nüsslein-Volhard, C. (2013). Genetic Lineage Labeling in Zebrafish Uncovers
999    Novel Neural Crest Contributions to the Head, Including Gill Pillar Cells.
1000    *Development*, 140(4), 916–925.

1001  Montoro, D. T. et al. (2018). A Revised Airway Epithelial Hierarchy Includes CFTR-
1002    Expressing Ionocytes. *Nature*, 560(7718), 319–324.

1003  Moran, D. T., Rowley III, J. C., Aiken, G. R. & Jafek, B. W. (1992). Ultrastructural
1004    Neurobiology of the Olfactory Mucosa of the Brown Trout, Salmo Trutta.
1005    *Microscopy Research and Technique*, 23(1), 28–48.

1006  Morrison, C. M. & Odense, P. H. (1978). Distribution and Morphology of the Rodlet
1007    Cell in Fish. *Journal of the Fisheries Board of Canada*, 35(1), 101–116.

1008  Mosimann, C., Puller, A.-C., Lawson, K. L., Tschopp, P., Amsterdam, A. & Zon, L. I.
1009    (2013). Site-Directed Zebrafish Transgenesis into Single Landing Sites with the
1010    PhiC31 Integrase System. *Developmental Dynamics*, 242(8), 949–963.

1011  Muller, J. F. & Marc, R. E. (1984). Three Distinct Morphological Classes of
1012    Receptors in Fish Olfactory Organs. *Journal of Comparative Neurology*, 222(4),
1013    482–495.

Nüsslein-Volhard, C. & Dahm, R. (2002). *Zebrafish: A Practical Approach*. Oxford: Oxford University Press.

Olivares, J. & Schmachtenberg, O. (2019). An Update on Anatomy and Function of the Teleost Olfactory System. *PeerJ*, 7, e7808.

Parisi, V., Guerrera, M. C., Abbate, F., Garcia-Suarez, O., Viña, E., Vega, J. A. & Germanà, A. (2014). Immunohistochemical Characterization of the Crypt Neurons in the Olfactory Epithelium of Adult Zebrafish. *Annals of Anatomy*, 196(4), 178–182.

Pinto, C. S., Khandekar, A., Bhavna, R., Kiesel, P., Pigino, G. & Sonawane, M. (2019). Microridges Are Apical Epithelial Projections Formed of F-Actin Networks That Organize the Glycan Layer. *Scientific Reports*, 9, 12191.

Portela-Gomes, G. M., Lukinius, A. & Grimelius, L. (2000). Synaptic Vesicle Protein 2, a New Neuroendocrine Cell Marker. *American Journal of Pathology*, 157(4), 1299–1309.

Raj, B., Wagner, D. E., McKenna, A., Pandey, S., Klein, A. M., Shendure, J., Gagnon, J. A. & Schier, A. F. (2018). Simultaneous Single-Cell Profiling of Lineages and Cell Types in the Vertebrate Brain. *Nature Biotechnology*, 36(5), 442–450.

Ramírez-Weber, F.-A. & Kornberg, T. B. (1999). Cytonemes : Cellular Processes That Project to the Principal Signaling Center in Drosophila Imaginal Discs. *Cell*, 97, 599–607.

Reid, L., Meyrick, B., Antony, V. B., Chang, L. Y., Crapo, J. D. & Reynolds, H. Y. (2005). The Mysterious Pulmonary Brush Cell: A Cell in Search of a Function. *American Journal of Respiratory and Critical Care Medicine*, 172(1), 136–139.

Reiten, I., Uslu, F. E., Fore, S., Pelgrims, R., Ringers, C., Diaz Verdugo, C., Hoffman, M., Lal, P., Kawakami, K., Pekkan, K., Yaksi, E. & Jurisch-Yaksi, N. (2017). Motile-Cilia-Mediated Flow Improves Sensitivity and Temporal Resolution of Olfactory Computations. *Current Biology*, 27(2), 166–174.

Rhein, L. D., Cagan, R. H., Orkand, P. M. & Dolack, M. K. (1981). Surface Specializations of the Olfactory Epithelium of Rainbow Trout, Salmo Gairdneri. *Tissue and Cell*, 13(3), 577–587.

Riedl, J., Crevenna, A. H., Kessenbrock, K., Yu, J. H., Neukirchen, D., Bista, M., Bradke, F., Jenne, D., Holak, T. A., Werb, Z., Sixt, M. & Wedlich-Soldner, R. (2008). Lifeact: A Versatile Marker to Visualise F-Actin. *Nature Methods*, 5(7),

605–607.

Rodrigues, F. S. L. M., Doughton, G., Yang, B. & Kelsh, R. N. (2012). A Novel Transgenic Line Using the Cre-Lox System to Allow Permanent Lineage-Labeling of the Zebrafish Neural Crest. *Genesis*, 50(10), 750–757.

Satija, R., Farrell, J. A., Gennert, D., Schier, A. F. & Regev, A. (2015). Spatial Reconstruction of Single-Cell Gene Expression Data. *Nature Biotechnology*, 33(5), 495–502.

Sato, Y., Miyasaka, N. & Yoshihara, Y. (2005). Mutually Exclusive Glomerular Innervation by Two Distinct Types of Olfactory Sensory Neurons Revealed in Transgenic Zebrafish. *Journal of Neuroscience*, 25(20), 4889–4897.

Saxena, A., Peng, B. N. & Bronner, M. E. (2013). Sox10-Dependent Neural Crest Origin of Olfactory Microvillous Neurons in Zebrafish. *eLife*, 2, e00336.

Schindelin, J., Arganda-Carreras, I., Frise, E., Kaynig, V., Longair, M., Pietzsch, T., Preibisch, S., Rueden, C., Saalfeld, S., Schmid, B., Tinevez, J.-Y., White, D. J., Hartenstein, V., Eliceiri, K., Tomancak, P. & Cardona, A. (2012). Fiji: An Open-Source Platform for Biological-Image Analysis. *Nature Methods*, 9(7), 676–682.

Schmid, B., Schindelin, J., Cardona, A., Longair, M. & Heisenberg, M. (2010). A High-Level 3D Visualization API for Java and ImageJ. *BMC Bioinformatics*, 11, 274.

Schneider, C., O'Leary, C. E. & Locksley, R. M. (2019). Regulation of Immune Responses by Tuft Cells. *Nature Reviews Immunology*, 19(9), 584–593.

Schulte, E. (1972). Untersuchungen an Der Regio Olfactoria Des Aals, Anguilla Anguilla L. *Zeitschrift für Zellforschung und Mikroskopische Anatomie*, 125, 210–228.

Sekerková, G., Zheng, L., Loomis, P. A., Changyaleket, B., Whitlon, D. S., Mugnaini, E. & Bartles, J. R. (2004). Espins Are Multifunctional Actin Cytoskeletal Regulatory Proteins in the Microvilli of Chemosensory and Mechanosensory Cells. *Journal of Neuroscience*, 24(23), 5445–5456.

Sola, C., Giulianini, P. G. & Ferrero, E. A. (1993). Ultrastructural Characterization of the Olfactory Organ in Glass Eels, Anguilla Anguilla (Osteichthyes, Anguilliformes). *Italian Journal of Zoology*, 60(3), 253–261.

Sui, P., Wiesner, D. L., Xu, J., Zhang, Y., Lee, J., Van Dyken, S., Lashua, A., Yu, C., Klein, B. S., Locksley, R. M., Deutsch, G. & Sun, X. (2018). Pulmonary Neuroendocrine Cells Amplify Allergic Asthma Responses. *Science*, 360(6393),

1082    eaan8546.

1083 Tang, W. & Bronner, M. E. (2020). Neural Crest Lineage Analysis: From Past to
1084    Future Trajectory. *Development*, 147, dev193193.

1085 Theriot, J. A. & Mitchison, T. J. (1991). Actin Microfilament Dynamics in Locomoting
1086    Cells. *Nature*, 352(6331), 126–131.

1087 Tilney, L. G., Derosier, D. J. & Mulroy, M. J. (1980). The Organization of Actin
1088    Filaments in the Stereocilia of Cochlear Hair Cells. *Journal of Cell Biology*,
1089    86(1), 244–259.

1090 Tsujikawa, M. & Malicki, J. (2004). Intraflagellar Transport Genes Are Essential for
1091    Differentiation and Survival of Vertebrate Sensory Neurons. *Neuron*, 42(5), 703–
1092    716.

1093 Wakisaka, N., Miyasaka, N., Koide, T., Masuda, M., Hiraki-Kajiyama, T. & Yoshihara,
1094    Y. (2017). An Adenosine Receptor for Olfaction in Fish. *Current Biology*, 27(10),
1095    1437–1447.

1096 Waryani, B., Zhao, Y., Zhang, C., Abbasi, A. R., Ferrando, S., Dai, R., Soomro, A.
1097    N., Baloch, W. A. & Abbas, G. (2015). Surface Architecture of the Olfactory
1098    Epithelium of Two Chinese Cave Loaches (Cypriniformes: Nemacheilidae:
1099    Oreonectes). *Italian Journal of Zoology*, 82(2), 179–185.

1100 Waryani, B., Zhao, Y., Zhang, C., Dai, R. & Abbasi, A. R. (2013). Anatomical Studies
1101    of the Olfactory Epithelium of Two Cave Fishes Sinocyclocheilus Jii and S.
1102    Furcodorsalis (Cypriniformes: Cyprinidae) from China. *Pakistan Journal of*
1103    *Zoology*, 45(4), 1091–1101.

1104 Wattrus, S. J. & Zon, L. I. (2020). A Transgenic System for Rapid Magnetic
1105    Enrichment of Rare Embryonic Cells. *Zebrafish*, 17(5), 354–357.

1106 Whitlock, K. E. (2015). The Loss of Scents: Do Defects in Olfactory Sensory Neuron
1107    Development Underlie Human Disease? *Birth Defects Research Part C -*
1108    *Embryo Today: Reviews*, 105(2), 114–125.

1109 Xiao, T., Roeser, T., Staub, W. & Baier, H. (2005). A GFP-Based Genetic Screen
1110    Reveals Mutations That Disrupt the Architecture of the Zebrafish Retinotectal
1111    Projection. *Development*, 132(13), 2955–2967.

1112 Yamamoto, M. & Ueda, K. (1978). Comparative Morphology of Fish Olfactory
1113    Epithelium - IV. *Bulletin of the Japanese Society of Scientific Fisheries*, 44(11),
1114    1207–1212.

1115 Zachar, P. C. & Jonz, M. G. (2012). Confocal Imaging of Merkel-like Basal Cells in

1116 the Taste Buds of Zebrafish. *Acta Histochemica*, 114(2), 101–115.

1117 Zhang, X.-Y., Huang, Z.-Q., Ning, T., Xiang, X.-H., Li, C.-Q., Chen, S.-Y. & Xiao, H.

1118 (2018). Microscopic and Submicroscopic Gradient Variation of Olfactory

1119 Systems among Six Sinocyclocheilus Species Living in Different Environments.

1120 *Zoological Society of Japan*, 35(5), 411–420.

1121